Prepared in cooperation with the Ministry of Petroleum, Energy and Mines, Islamic Republic of Mauritania

Second Projet de Renforcement Institutionnel du Secteur Minier de la République Islamique de Mauritanie (PRISM-II)

Mineral Potential for Incompatible Element Deposits Hosted in Pegmatites, Alkaline Rocks, and Carbonatites in the Islamic Republic of Mauritania:

Phase V, Deliverable 87

By Cliff D. Taylor and Stuart A. Giles

Open-File Report 2013–1280 Chapter Q

U.S. Department of the Interior
U.S. Geological Survey

U.S. Department of the Interior
SALLY JEWELL, Secretary

U.S. Geological Survey
Suzette M. Kimball, Acting Director

U.S. Geological Survey, Reston, Virginia: 2015

For more information on the USGS—the Federal source for science about the Earth, its natural and living resources, natural hazards, and the environment—visit http://www.usgs.gov or call 1–888–ASK–USGS

For an overview of USGS information products, including maps, imagery, and publications, visit http://www.usgs.gov/pubprod

To order this and other USGS information products, visit http://store.usgs.gov

Suggested citation:
Taylor, C.D., and Giles, S.A., 2015, Mineral potential for incompatible element deposits hosted in pegmatites, alkaline rocks, and carbonatites in the Islamic Republic of Mauritania (phase V, deliverable 87), chap. Q *of* Taylor, C.D., ed., Second projet de renforcement institutionnel du secteur minier de la République Islamique de Mauritanie (PRISM-II): U.S. Geological Survey Open-File Report 2013–1280-Q, 41 p., http://dx.doi.org/10.3133/ofr20131280. [In English and French.]

Multiple spellings are used in various literatures, and may be reflected in the text.

This report is preliminary and has not been reviewed for conformity with U.S. Geological Survey editorial standards or for stratigraphic nomenclature.

The report is being released in both English and French. In both versions, we use the French-language names for formal stratigraphic units.

ISSN 2331-1258 (online)

Conversion Factors

SI to Inch/Pound

Multiply	By	To obtain
	Length	
centimeter (cm)	0.3937	inch (in.)
millimeter (mm)	0.03937	inch (in.)
decimeter (dm)	0.32808	foot (ft)
meter (m)	3.281	foot (ft)
kilometer (km)	0.6214	mile (mi)
	Area	
hectare (ha)	2.471	acre
square meter (m^2)	0.0002471	acre
square kilometer (km^2)	0.3861	square mile (mi^2)
	Volume	
cubic kilometer (km^3)	0.2399	cubic mile (mi^3)
	Mass	
gram (g)	0.03527	ounce, avoirdupois (oz)
kilogram (kg)	2.205	pound avoirdupois (lb)
megagram (Mg)	1.102	ton, short (2,000 lb)
megagram (Mg)	0.9842	ton, long (2,240 lb)
metric ton per day	1.102	ton per day (ton/d)
megagram per day (Mg/d)	1.102	ton per day (ton/d)
metric ton per year	1.102	ton per year (ton/yr)
	Pressure	
kilopascal (kPa)	0.009869	atmosphere, standard (atm)
kilopascal (kPa)	0.01	bar
	Energy	
joule (J)	0.0000002	kilowatt hour (kWh)

ppm, parts per million; ppb, parts per billion; Ma, millions of years before present; m.y., millions of years; Ga, billions of years before present; 1 micron or micrometer (µor µm) = 1 × 10-6 meters; Tesla (T) = the field intensity generating 1 Newton of force per ampere (A) of current per meter of conductor

Temperature in degrees Celsius (°C) may be converted to degrees Fahrenheit (°F) as follows:

°F=(1.8×°C)+32

Temperature in degrees Fahrenheit (°F) may be converted to degrees Celsius (°C) as follows:

°C=(°F-32)/1.8

Coordinate information is referenced to the World Geodetic System (WGS 84)

Acronyms

AMT	Audio-magnetotelluric
ASTER	Advanced Spaceborne Thermal Emission and Reflection Radiometer
AVIRIS	Airborne Visible/Infrared Imaging Spectrometer
BIF	Banded iron formation
BLEG	Bulk leach extractable gold
BGS	British Geological Survey
BRGM	Bureau de Recherches Géologiques et Minières (Mauritania)
BUMIFOM	The Bureau Minier de la France d'Outre-Mer
CAMP	Central Atlantic Magmatic Province
CGIAR-CSI	Consultative Group on International Agricultural Research-Consortium for Spatial Information
DEM	Digital Elevation Model
DMG	Direction des Mines et de la Géologie
EMPA	Electron Microprobe Analysis
EM	Electromagnetic (geophysical survey)
EOS	Earth Observing System
eU	Equivalent uranium
GGISA	General Gold International
GIF	Granular iron formation
GIFOV	Ground instantaneous field of view
GIS	Geographic Information System
HIF	High grade hematitic iron ores
IHS	Intensity/Hue/Saturation
IAEA	International Atomic Energy Agency
IOCG	Iron oxide copper-gold deposit
IP	Induced polarization (geophysical survey)
IRM	Islamic Republic of Mauritania
JICA	Japan International Cooperation Agency
JORC	Joint Ore Reserves Committee (Australasian)
LIP	Large Igneous Province
LREE	Light rare-earth element
METI	Ministry of Economy, Trade and Industry (Japan)
MICUMA	Société de Mines de Cuivre de Mauritanie
MORB	Mid-ocean ridge basalt
E-MORB	Enriched mid-ocean ridge basalt
N-MORB	Slightly enriched mid-ocean ridge basalt
T-MORB	Transitional mid-ocean ridge basalt
Moz	Million ounces
MVT	Mississippi Valley-type deposits
NASA	United States National Aeronautics and Space Administration
NLAPS	National Landsat Archive Processing System
OMRG	Mauritanian Office for Geological Research
ONUDI	(UNIDO) United Nations Industrial Development Organization

PRISM	Projet de Renforcement Institutionnel du Secteur Minier
PGE	Platinum-group elements
RC	Reverse circulation drilling
REE	Rare earth element
RGB	Red-green-blue color schema
RTP	Reduced-to-pole
SARL	Société à responsabilité limitée
SEDEX	Sedimentary exhalative deposits
SNIM	Société National Industrielle et Minière (Mauritania)
SP	Self potential (geophysical survey)
SRTM	Shuttle Radar Topography Mission
SWIR	Shortwave infrared
TISZ	Tacarat-Inemmaudene Shear Zone
TM	Landsat Thematic Mapper
UN	United Nations
UNDP	United Nations Development Program
US	United States
USA	United States of America
USGS	United States Geological Survey
UTM	Universal Transverse Mercator projection
VHMS	Volcanic-hosted massive sulfide
VisNIR	Visible near-infrared spectroscopy
VLF	Very low frequency (geophysical survey)
VMS	Volcanogenic massive sulfide deposit
WDS	Wavelength-dispersive spectroscopy
WGS	World Geodetic System

Mineral Potential for Incompatible Element Deposits Hosted in Pegmatites, Alkaline Rocks, and Carbonatites in the Islamic Republic of Mauritania

Summary

Review of PRISM-I documents and the National inventory of mineral occurrences suggests that resources of U, Th, Nb, Ta, Be, rare earth elements (REEs) and fluorite are known in Mauritania and have been exploited in the past at the Bou Naga alkaline complex. Several different deposit types are indicated by the available data. Pegmatitic veins are recorded in several areas of the Archean and Paleoproterozoic portions of the Rgueïbat Shield and are prospective for resources of Li, Be, Nb, Ta, U, Th, and REEs. Over 150 beryl pegmatites are known in the Khnefissat and Inkebden areas of the Chami greenstone belt, and additional concentrations of pegmatites are known in the Guelb Nich Sud area of the Sebkhet Nich greenstone belt and in the northeastern part of the Amsaga Complex. Due to the small size of these deposits, they are unlikely to be economic unless additional value can be gained by processing contained minerals for their industrial uses.

Potential for incompatible element deposits associated with alkaline granites, syenites, and phonolites of the Tigsmat el Khadra Complex exists in the Paleoproterozoic portion of the Rgueïbat Shield in northern and northeastern Mauritania. The small alkaline complex at Tabatanet is associated with a magnetic and radiometric anomaly and consists of a probable vein-type deposit that extends for 500 m. The hyperalkaline granite at Tigsmat may have REE enrichments in associated placers but appears to be of low potential. Two other areas at el Mrhader and at el Hajar have indications of potential based on geophysics and high scintillometer readings. All of these prospects and past mining at Bou Naga indicate potential for mineralization related to alkaline igneous rocks.

A third major possibility for U, Th, REE, and other incompatible elements exists in association with carbonatite complexes, known to be present in Mauritania. Deposits of this type can host a wide array of valuable metals and industrial minerals (for example, Phalabora carbonatite complex, South Africa; Hicks Dome carbonatite complex and associated fluorite deposits of the Illinois-Kentucky Fluorspar District of the U.S. Midcontinent) and are most common in cratonic areas that have undergone rifting. PRISM-I studies suggest the presence of a carbonatite at Guelb er Richat and a coincident high thorium geophysical anomaly. The co-location of Guelb er Richat on prominent ENE trending structures with two separate swarms of kimberlite intrusions suggest that this structure is seated in the sub-Taoudeni cratonic basement and could localize the emplacement of additional carbonatite (and kimberlite) bodies.

USGS review of PRISM-I data suggests that there is abundant documentation of the Bou Naga alkaline complex and to a lesser degree, the Guelb er Richat carbonatite complex, but that all other occurrences of U, Th, REE, and associated elements are poorly described, and poorly understood (Taylor, 2007).

Contents

Figures

Tables

Second Projet de Renforcement Institutionnel du Secteur Minier de la République Islamique de Mauritanie (PRISM-II)

Mineral Potential for Incompatible Element Deposits Hosted in Pegmatites, Alkaline Rocks, and Carbonatites in the Islamic Republic of Mauritania:

Phase V, Deliverable 87

By Cliff D. Taylor[1] and Stuart A. Giles[1]

1 Introduction

Most deposits of the incompatible elements U, Th, rare earth elements (REE), Nb, Ta, and Be, the mineral fluorite, and other industrial minerals are igneous in origin. Three major types of igneous rocks that host these commodities are present in Mauritania and have the potential to contain economic deposits. Mineral deposits containing these commodities are hosted in pegmatites, alkaline igneous complexes, and carbonatites.

Pegmatites form as late stage differentiates during crystallization of felsic igneous intrusions and as leucogranite segregations and veins during recrystallization of metamorphic rocks of a wide range of compositions that have undergone melting during very high grade regional metamorphic events. As these granitic melts cool and crystallize, common rock-forming minerals grow from chemical elements in the magma. Chemical elements that don't fit into the growing mineral's atomic structure, because the atoms are too large or don't have the right electrical charge, remain in the residual melt and concentrate in the late-stage silicon-rich fluid. This fluid sometimes crystallizes as a granitic rock called pegmatite, which is composed of large mineral crystals of quartz and feldspar and that often include beryl, tourmaline, and other exotic minerals that can contain economic concentrations of rare earth elements (REE) and other valuable incompatible elements. When of sufficient quality, some of these minerals have value as gems and semi-precious stones.

Alkaline complexes are composed of alkaline granites, syenites, alkaline gabbros, diorites, and their extrusive equivalents such as rhyolites (pantellerites), trachytes, and phonolites. They tend to form at continental margins and within cratonic areas where incipient rifting initiates partial melting at the base of the crust. Low degrees of partial melting result in the production of small batches of magma into which highly incompatible elements are strongly partitioned. Resulting mineral deposits can thus

[1]U.S. Geological Survey, Denver Federal Center, Denver, Colorado 80225 U.S.A.

contain economic concentrations of U, Th, REEs, Nb, Ta, fluorine and other valuable commodities.

Carbonatites, often associated with kimberlites, are special cases where rifting in cratonic areas initiates melting beneath very thick crust. Resulting magmas can be CO_2 saturated, producing concentrations of igneous carbonate, apatite, uraninite, thorite, and Nb-, Ta-, Ce-, REE-bearing phases. Although much rarer than pegmatites and alkaline igneous complexes, they are host to some of the greatest deposits of U, Th, and REE bearing minerals in the Earth's crust. Major world class mineral deposits in carbonatites include the Phalabora Complex in South Africa and the Bayan Obo Complex in China.

4.1 Pegmatites and Pegmatitic Veins of the Rgueïbat Shield

The Rgueïbat Shield in northwestern Mauritania consists of the exposed Archean portion of the West African Craton. Recent mapping by the British Geological Survey (BGS) divides this part of the shield into two terranes separated by a major north-northeast trending shear zone (Pitfield and others, 2004; O'Connor and others, 2005). The eastern Choum-Rag el Abiod terrane consists primarily of granulite facies metamorphic rocks of the Amsaga Complex that are cut by major granitic and less commonly by mafic-ultramafic bodies, all of which range in age from 3,000 to 2,700 Ma. Older fragments of preserved crustal material consisting of greenstone remnants in migmatitic gneisses are probably about 3,200 Ma in age. This region is interpreted as the dismembered and reworked root zone of a typical granite-greenstone assemblage (Gunn and others, 2004). The western Tasiast-Tijirit terrane consists of a typical Archean granite-greenstone assemblage exposed at shallower levels than the Choum-Rag el Abiod terrane and are thus much less sheared and tectonized than the similar-age rocks to the east. The oldest rocks are variably migmatized tonalitic gneisses that are cut by younger granitic phases and tectonically or unconformably underlie the greenstone belts (fig. 1).

The main greenstone belts in the Tasiast-Tijirit terrane are named, from east to west, the Tijirit, Ahmeyim, Sebkhet Nich, Kreidat, and Chami greenstone belts. Two smaller greenstone belts to the west of the Chami belt are called the Hadeibt Agheyâne and Hadeibt Lebtheinîyé greenstone belts and are collectively referred to as the Lebzenia greenstone belts (fig. 1). These greenstone belts consist predominantly of mafic metavolcanic and siliciclastic metasedimentary rocks metamorphosed at low- to medium-grades. Banded iron formation and ultramafic rocks are locally common and intermediate to felsic metavolcanic rocks are rare. The greenstone belts are locally intensely sheared especially along competency contrasts between lithologic units, and major ductile shear zones control both the current shape of the belts as well as folds within the belts. The most common intrusive rock in the Tasiast-Tijirit terrane is a biotite-granodiorite or tonalite that forms very large plutons within and marginal to the greenstone belts. The youngest intrusive rocks in the terrane consist of a series of small intrusions consisting of coarse-grained to pegmatitic muscovite granite that are present in the Kriedat, Chami, and Sebkhet Nich belts. These intrusions are leucocratic and are dominated by quartz and white feldspar with accessory muscovite. However, a pegmatitic phase, usually forming sheets and sharply defined veins up to 1 meter thick, is present and contains a suite of lithium-, strontium-, and beryllium-bearing minerals as well as tourmaline, biotite, garnet, and opaque minerals. Muscovite books in these pegmatites are up to 1 meter in

length. These muscovite-pegmatites are locally strongly fractured (Gunn and others, 2004).

Gunn and others (2004) have summarized the known occurrences and exploration history of pegmatites in the Rgueïbat Shield of northwestern Mauritania. They state that several Li- and Be-bearing pegmatites were discovered in the 1960s by the Bureau de Recherches Géologiques et Minières (BRGM) but that the economic potential for the known occurrences is low. At most, a few occurrences may contain a few tens of tonnes of beryl and that several others may contain up to 10 tonnes of spodumene or lepidolite. Pegmatites are known in five areas: the Kriedat, Chami, and Sebkhet Nich greenstone belts of the Tasiast-Tijirit terrane, the Tamagot window in the southwestern Inchiri district, and the Iguilid metagabbro in the northern Amsaga Complex of the Choum-Rag el Abiod terrane. The lithologic and stratigraphic terminology used for rock units of the northwestern Rgueïbat Shield in this report are presented in Figure 2 (Gunn and others, 2004). The locations of the southern Tasiast-Tijirit terrane, Amsaga Complex, Iguilid Massif, Bou Naga alkaline complex and other features discussed in the text are shown in figure 3.

4.1.1 Pegmatite Veins of the Tasiast-Tijirit Terrane

Over 150 pegmatitic beryl occurrences were reported by the BGS in the Khnefissat area of the north-western Chami greenstone belt (Gunn and others, 2004). They are described as pegmatitic veins 2–4 m thick that are traceable for several hundred meters as networks of both horizontal and vertical veins cutting fractured amphibolite. Their mineralogy is dominantly quartz, albite, oligoclase, microcline, perthite, with minor biotite, muscovite, epidote and trace magnetite. Garnet, beryl, columbite, spodumene, lepidolite, clevelandite, tourmaline and rose beryl are minor constituents. Pegmatitic aplite and albitite veins have been observed accompanying the more typical pegmatite veins. The pegmatitic veins are unmineralized, however the albitite veins are often highly mineralized and consist of relatively undeformed veins of quartz, albite, spessartine, and muscovite with widespread beryl and local concentrations of spodumene, lepidolite, and columbo-tantalite. Recent trenching at Khnefissat indicates commercial exploration activity in a 1-kilometer-long zone along the edge of a granite body. The occurrence of quartz-feldspar pegmatites containing locally abundant green mica and sporadic tourmaline, lepidolite, and garnet is reported, however no knowledge of analytical results are available (Gunn and others, 2004).

Pegmatite vein ocurrences of similar description are also found at Timmimichat and Inkebden in the northeastern and southwestern Chami belt, respectively, at the Guetel Khaye, and Sineine occurrences in the Kriedat belt, and at Guelb Nich Sud in the southeastern portion of the Sebkhet Nich greenstone belt. Host rocks at all of the pegmatite occurrences in the Tasiast-Tijirit terrane consist of Mesoarchean supracrustal rocks of the Lebzenia Group, the Tasiast Suite, and the undivided mafic metavolcanic rocks and amphibolites of the LbB unit (figs. 1–3).

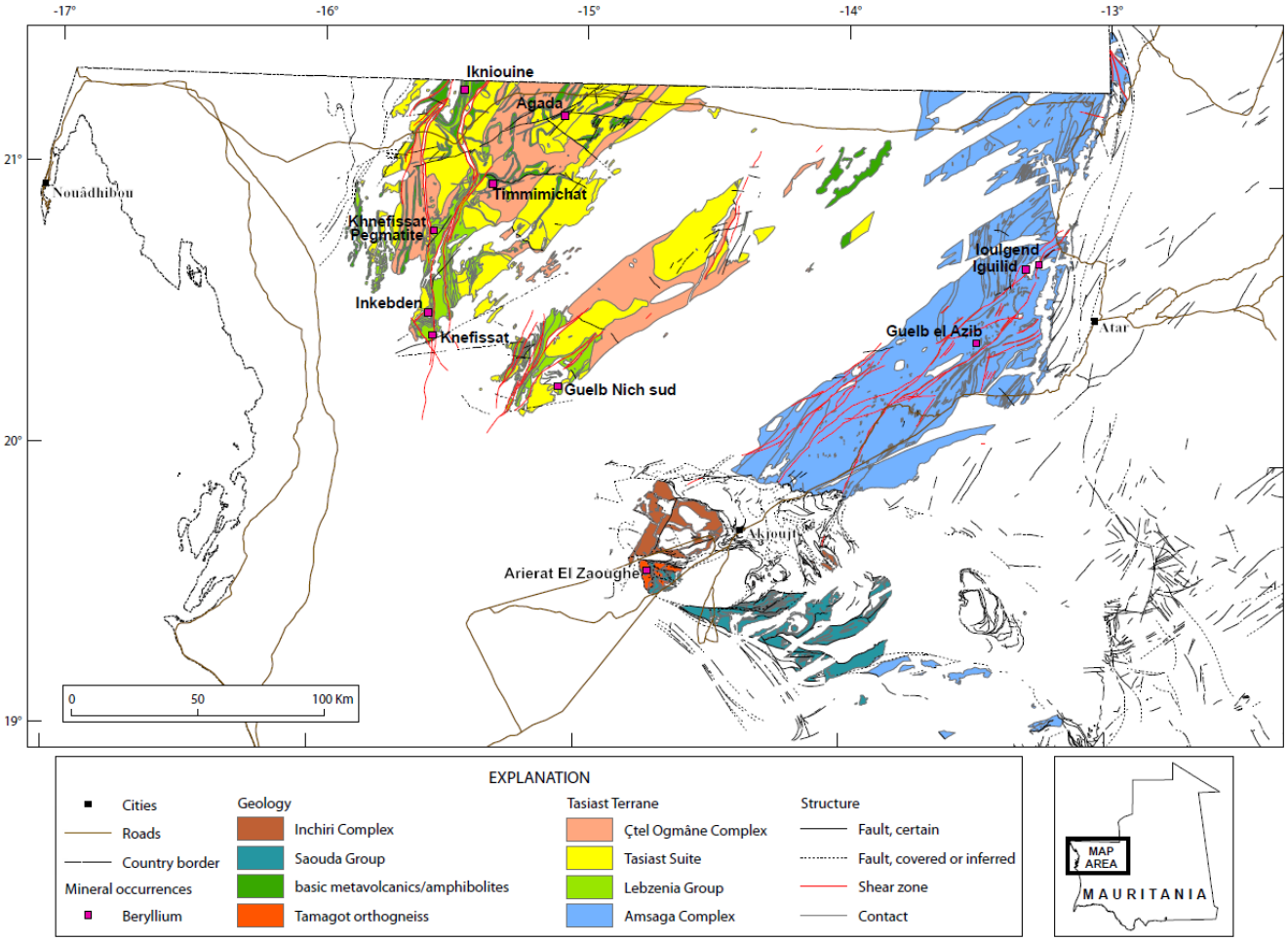

Figure 1. Simplified geologic map of the northwestern Rgueïbat Shield showing the Choum-Rag el Abiod and Tasiast-Tijirit terranes. The principal greenstone belts and locations of pegmatite occurrences discussed in the text are shown.

Tasiast-Tijirit Terrane				Choum-Rag El Abiod Terrane	
Unassigned	Mylonite; ductile melange; quartz-epidote rock			Unassigned	Mylonite; tectonically interlayered rocks
Lebzenia Group	Aouéoua Formation (metavolcanics 2960 Ma)	Talhayet Formation	Metamorphosed supracrustal rocks	Saouda Group Amsaga Complex	Greenstones; banded iron formation; quartzite; carbonate rocks; felsic metavolcanics. Amphibolites; banded iron formation; various quartzofeldspathic gneisses; sillimanite-cordierite-garnet-gneiss; hypersthene-charnockites; carbonate rocks; quartzites
	Sebkhet Nich Formation	Tijraj Formation			
	Gabbro; microgabbro; anorthosite; ultrabasic rock; pyroxenite; sodalite-syenite		Intrusive rocks		Dunite-carbonate breccia ; gabbro, microgabbro, anorthosite, ultrabasic rock, serpentinite, metagabbro, metamicrogabbro; pegmatite.
Tasiast Suite	Leucogranite; pegmatitic muscovite-granite; xenolithic mafic-granite; porphyritic microgranite			Iguilid Suite	2706±54 Ma
				Touijenjert--Modreigue Suite	2726±7 Ma
				Tacarat Suite	
	Biotite-granodiorite; porphyritic granodiorite; foliated biotite-granodiorite; xenolithic biotite-granodiorite gneissic biotite-granodiorite;			Aoutitilt Suite (synchronous with ductile shearing within the 'Flower structure)	2954±11 Ma
	Bir Igueni granite (2933±16 Ma)			Tonalitic migmatitic gneiss; tonalitic gneiss	
	Epidote-granodiorite; Gleibat El Fhoud Sub-suite (2912±36 Ma)				
	Granite				
Çtel Ogmâne Complex	Agmatitic and nebulitic migmatitic gneiss; stromatic migmatitic gneiss; migmatitic gneiss.				

Figure 2. Lithologic and stratigraphic terminology and age relationships of rock units in the northwestern Rgueïbat Shield (from Gunn and others, 2004).

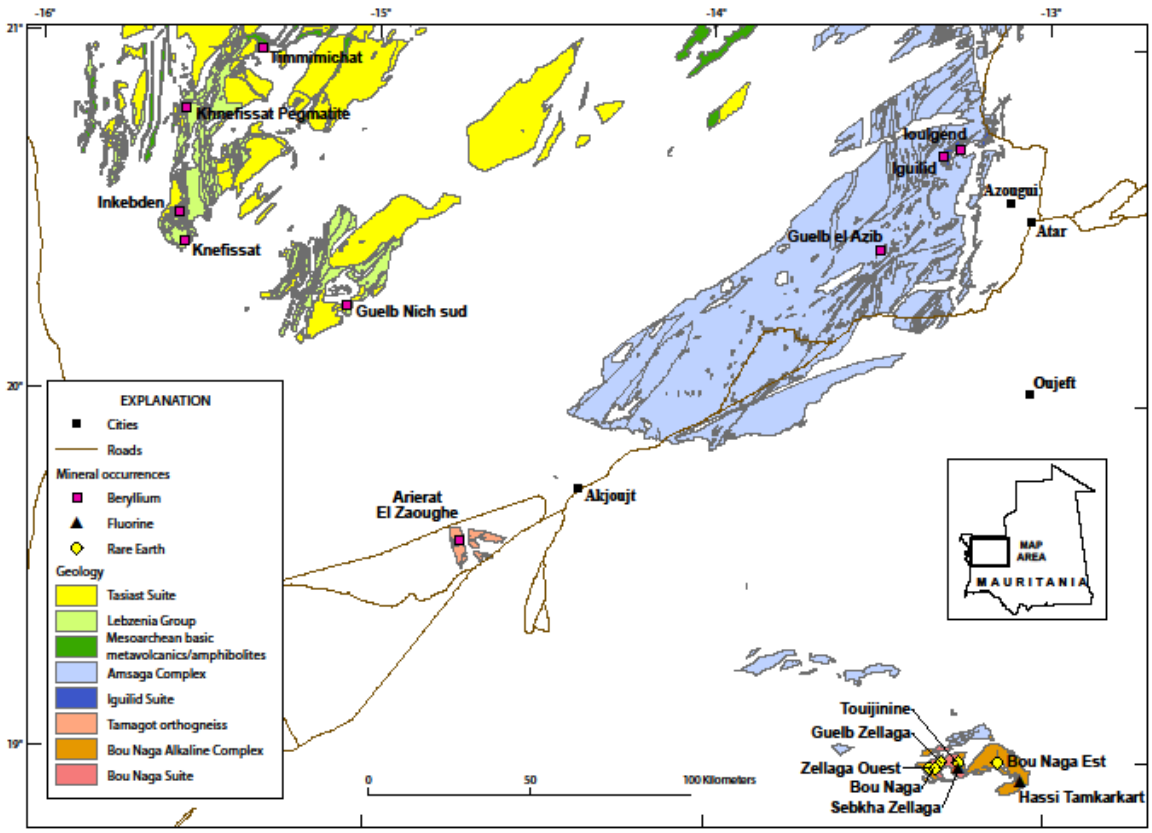

Figure 3. Simplified geologic map showing the location of the southern Tasiast-Tijirit terrane, Amsaga Complex, Iguilid Massif, Bou Naga alkaline complex and other features discussed in the text.

4.1.2 Pegmatite Veins of the Tamagot Window and the Northern Amsaga Complex

Vein pegmatite occurrences similar to those in the Tasiast-Tijirit terrane are also present in the Tamagot orthogneiss in a tectonic window southwest of Akjoujt, and in the Iguilid massif of the northeastern Amsaga Complex (fig. 3). The Tamagot window is an area of Archean rocks on the southwest side of the Akjoujt nappe pile consisting of a granite-greenstone assemblage similar to that observed in the Tasiast-Tijirit terrane. The Tamagot Complex consists of amphibole-garnet bearing, granitic gneiss and migmatite of the Tamagot orthogneiss. Greenschist facies Mesoarchean metavolcanic rocks of the Saouda Group are synformally infolded with amphibolite-facies granitic gneisses of the Tamagot orthogneiss (Pitfield and others, 2004). Late-stage pegmatite veins cut the Tamagot orthogneiss as in the Tasiast-Tijirit terrane.

In the northern Amsaga Complex, beryl occurrences are located in two areas; Guelb el Azid and Iguilid (fig. 3). Very little is known about Guelb el Azid where beryl is reported in pegmatitic veins (?) in a hypersthene-bearing migmatitic gneiss. At Iguilid, pegmatite veins occur in metagabbroic rocks of the Iguilid massif (2,706 Ma; Pitfield and others, 2004). The Iguilid massif is the largest of a series of metagabbro intrusive bodies located throughout the Amsaga Complex. It consists of an arcuate body elongated in the

N-S direction underlying a range of large hills. Smaller metagabbro pods are common in the tectonically interleaved gneisses surrounding the intrusion and all of the metagabbroic rocks in the area are collectively referred to as the Iguilid Suite. The metagabbros are massive, equigranular, medium to coarse-grained, and weather to either a blue-gray or brown color. The Iguilid massif is cut by tourmaline and muscovite-bearing quartz-feldspar pegmatite veins and sheets similar to those occurring in the Tasiast-Tijirit terrane (Pitfield and others, 2004). Gunn and others (2004) describe 15 veins in the area, 12 of which contain beryl. They are relatively undeformed and contain quartz, feldspar, muscovite, tourmaline and garnet with sporadic crystals of blue beryl up to a few tens of centimeters (cm) in size, and minor magnetite, columbo-tantalite, apatite and scheelite.

4.2 Alkaline Intrusions in the Paleoproterozoic Portion of the Rgueïbat Shield

The northeastern Rgueïbat Shield is composed of Paleoproterozoic (Birimian) to Neoproterozoic granitoids and supracrustal rocks of the West African Craton. This region is characterized by a series of volcano-sedimentary belts and associated batholithic-scale granitic intrusive suites emplaced during the Eburnean orogeny from about 2,150–2,000 Ma. Two major sets of shear zones are present oriented NNW-SSE and E-W that often bound the volcano-sedimentary belts and (or) batholiths and localize late-crystallizing peralkaline granite and syenite intrusions as well as Jurassic dikes (Lahondère and others, 2003). These alkaline to hyperalkaline intrusions are recognized as the youngest rocks related to the Eburnean cycle and represent targets for possible U, Th, REE, F, and other incompatible element mineral occurrences.

Several occurrences are known in the northern and eastern Rgueïbat Shield within the alkaline Tigsmat el Khadra Suite. The Tigsmat el Khadra Suite consists of as many as ten separate small, roughly circular intrusions emplaced primarily within the late Birimian Adam Esseder Complex. The intrusions are present in two areas. The first area is located about 60 km (km) north of the town of Bir Moghreïn in the Bir Moghreïn 1:200,000 scale geologic map and contains the Tabatanate granite-syenite and the Gara El Hamouïed syenite bodies (fig. 4). The second area consists of a series of at least 8 intrusions near the eastern edge of the Adam Esseder Complex and at the contact between the Adam Esseder and Tin Bessaïs Complexes. These intrusions define a NNW-trending belt approximately 225 km long, or nearly the entire width of the northeastern Rgueïbat Shield, and are located (from SSE to NNW) in the Blekhzaymat, Tigsmat, El Hassan Ould Hamed, and Ain Ben Tili 1:200,000 scale geologic maps (Lahondère and others, 2003). These intrusions include the aegirine granites of Assif Msérif and Tigsmat el Khadra, the Hassi el Fogra syenite, and the Bir Lefjah phonolite (fig. 4). In general, these intrusions are visible on satellite images. However, in the field they exhibit poor exposure and have either no morphological expression or are represented in one or several small guelbs (Arabic for “hills). The intrusives generally exhibit microcrystalline, porphyritic, often fluidal and occasionally pegmatitic textures suggesting emplacement at high levels in the crust (Lahondère and others, 2003).

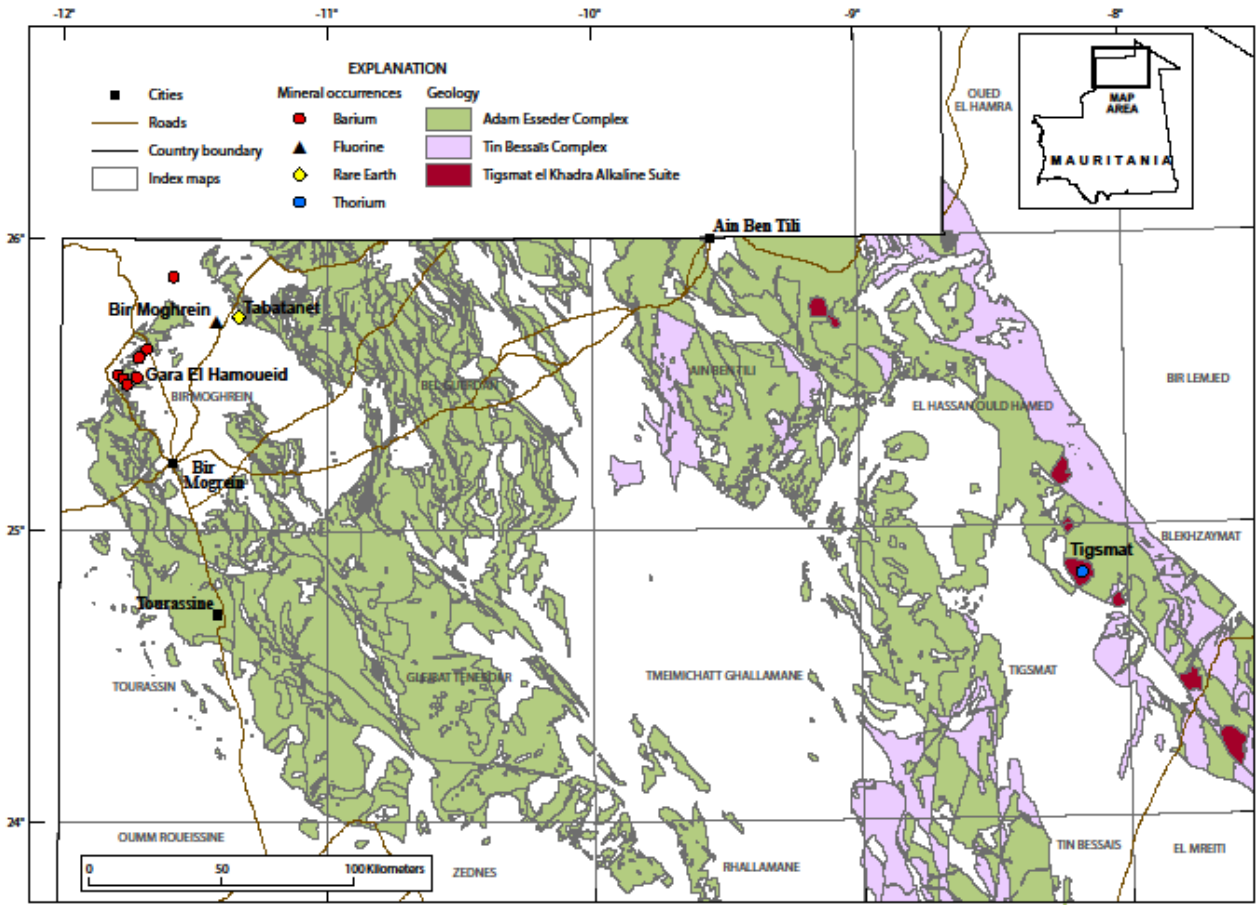

Figure 4. Simplified geology of the northeastern Rgueïbat Shield showing locations of features discussed in text.

The Tabatanate occurrence is located in the northeastern portion of the Bir Moghreïn 1:200,000 scale geologic map and is described as being hosted by small semicircular intrusion approximately 3 km in diameter that is exposed in about ten small guelbs that rise above the regolith. The intrusion consists of porphyritic granite, syenite, syenodiorite/syenogabbro, microsyenite, and microsyenite with foyaitic textures (Lahondère and others, 2003). The complex at Tabatanet is associated with magnetic and radiometric anomalies and consists of a probable dike-like deposit oriented east-west and extending for 500 m. Marot and others (2003) describe a late intrusive phase associated with this anomaly that has a microporphyritic and highly fluidal texture with mm-scale plagioclase laths, acicular pyroxenes or amphiboles, light brown carbonate, epidote, and possible allanite and cancrinite. Minor magnetite, pyrite (<1 percent), and sodalite (<2 percent) occurs in the cores of globules or vacuoles in the microgranite. Rocci (1960) describes the presence of numerous dikes generally several decimeters in thickness. Accessory zircon, sphene, and more rarely apatite and fluorite are also reported. In a study of about 50 heavy mineral concentrates from the area of the guelbs, hematite, ilmenite, magnetite, melanite garnet, pyroxene and amphibole, oxidized pyrite, rutile, and zircon are always present, monazite is present in 75 percent of the concentrates, 50 and

30 percent of the concentrates contain pink garnets and brown tourmaline, respectively, and minerals less commonly encountered include anatase, andalusite, anhydrite, barite, chrysoberyl, fluorite, sillimanite, spinel, and staurolite. Analcime is reported in thin section (Rocci, 1960). The BRGM sampling in the area indicates elevated REE contents. The site is also permissive for the occurrence of carbonatite (Marot and others, 2003). Listed as an alluvial REE occurrence related to the intrusion in the Mauritanian National Occurrences Database (Marsh and Anderson, 2015), it is likely that the designation of the occurrence is related to the heavy mineral concentrate sampling of Rocci (1960) over 50 years ago and there are no additional data to suggest whether the occurrence has economic significance.

The Bir Moghrein fluorite occurrence is listed as an alluvial surface on granite of the Adam Esseder Complex approximately 8.5 km west-southwest of Tabatanat. The Mauritanian National Occurrences Database (Marsh and Anderson, 2015) indicates that a heavy mineral concentrate processed from this site contains fluorite, pink octahedral zircons, sphene, brown garnets, ilmenite, epidote, oxidized pyrite, apatite, and rare tourmaline, martite, magnetite, pyroxenes and amphiboles, and rutile. This occurrence is also probably related to sampling performed by Rocci (1957, 1960) and there are no additional data to suggest whether the occurrence has economic significance.

The Gara El Hamouïed syenite body is located in the west-central portion of the Bir Moghrein 1:200,000-scale geologic map at the unconformity between the Rgueïbat Shield and overlying sedimentary rocks of the Black Zenmour sub-basin. It is approximately 48 km west-southwest of the Tabatanat intrusion. The intrusion is approximately 6.5 × 1–2 km in size and is elongate in an east-northeast direction parallel to the margin of the basin. Almost no written information is available. BRGM mapping identifies the intrusion as an aegirine syenite belonging to the Tigsmat el Khadra Suite (Lahondère and others, 2003). It appears to have an intrusive contact with granitic rocks of the Adam Esseder Complex, specifically the Bir En Nar granititic facies (described below), along its eastern margin and is in contact with Ordovician sedimentary rocks along its western margin. There are six separate epithermal vein barite-fluorite occurrences of the same name that are spatially associated with the intrusion. Two are immediately adjacent to the intrusion and the four others are approximately 2, 5, 6, and 11 km to the southeast, east, and northeast of the intrusion. All of the Gara El Hamouïed occurrences have exactly the same description and are described as quartz-barite-fluorite-sulfide veins 0.2–1.0 meter thick and up to 200 m in length that are discontinuously exposed over 2 to 3 km. They crosscut both the Precambrian basement of the shield as well as the overlying Ordovician sedimentary rocks on trends of north-south and NNE-SSW (Marsh and Anderson, 2015). They are interpreted to be related to Mauritanide orogenesis, however their genetic origins and relationship to the Gara El Hamouïed syenite body are unclear.

The aegirine granite at Tigsmat el Khadra in the northeastern Rgueïbat Shield is exposed in a group of guelbs of the same name. The guelbs are of low relief, rise slightly above the regolith surface, and are composed of light-colored, beige to white, medium-crystalline granite. The most noticeable feature of the granite is radiating clusters of mm-scale prismatic aegirine associated with alkali feldspar and amphibole and lesser plagioclase, quartz, Fe-Ti oxides, large zircons, sphene, and apatite. A decimeter-scale fine-grained, gray-colored dike of similar mineralogy was observed crosscutting the

margin of the aegirine granite (Lahondère and others, 2003). Marot and others (2003) suggest that the Tigsmat occurrence may have REE and rare metal enrichments in associated placers but appears to be of low potential. Host rocks at the occurrence consist of banded agpaitic granite and pegmatite bodies with infillings of quartz, amphibole, and other ferromagnesian minerals. The latest intrusive phase of the granite occurs as microcrystalline granitic dikes injected into the overlying pile of ignimbrites, however, low scintillometer readings obtained for the pegmatites and microgranite dikes (<180 counts/second (c/s)) suggest that they are not strongly mineralized.

The Assif Msérif aegirine granite intrusion is located about 18 km southeast of the Tigsmat occurrence and consists of two ovoid bodies several kilometers in size that are distinguished as radiometric anomalies confirmed by geochemical analyses (U and Th = 30 and 128 ppm, respectively; Lahondère and others, 2003). In outcrop the granite is heterogeneous with the dominant phase consisting of a medium-grained, white, quartz-feldspar-magnetite granite with local reddening due to the alteration of magnetite. The granite is cut by a complex series of later dikes that are often pegmatitic and marked by the presence of amazonite that has been exploited by artisanal miners. To the south the intrusive masses are in contact with granodiorites and tonalities of the Tin Bessaïs Complex and the northern margin is characterized by a brecciated contact with porphyritic microgranite (Lahondère and others, 2003). The northern contact is marked by two narrow intrusive facies that exhibit pronounced reddening and consist of a leucocratic microgranite adjacent to the main quartz-feldspar-magnetite granite and a facies composed of a medium-crystalline granite containing amphibole. The contact zone between these two facies is rich in coarse-crystalline amphiboles and is cut by injections of white-gray, microcrystalline granite containing fine-crystalline amphibole alternating with pegmatites containing amphibole crystals up to 3 cm in size. BRGM geologists note a similarity with coarse crystalline syenites of the Hassi el Fogra intrusion and suggest that there is a relationship between the granitic and syenitic intrusive facies of the intrusion. The shallow level of emplacement in the crust and presence of late-crystallizing phases suggests the potential for the existence of phases enriched in incompatible elements (Lahondère and others, 2003).

The Bir Lefjah phonolite body is located in the northeastern part of the Ain Ben Tili 1:200,000 geologic map and is best delineated as a roughly oblong mass about 15 km long and 8 km wide at its widest point based on satellite imagery. Two closely associated igneous phases have been identified in poor outcrop and consist of a slightly porphyritic apple-green fluidal textured lava containing amphibole and feldspar phenocrysts and quartz-pyrite-filled amygdules, and a gray microcrystalline rock with amphibole and possible pyroxene. Locally the microdiorite is cut by a meter-thick trachyandesite dike. Limited geochemical analyses and the presence in thin section of feldspathoid minerals (possibly analcime) confirm the undersaturated nature of the Bir Lefjah phonolite (Lahondère and others, 2003).

The Hassi el Fogra syenite intrusion is a circular body about 7 km in diameter that overlaps the edges of the El Hassan Ould Hamed and Oued El Hamra 1:200,000 scale geologic maps at the corner where the national boundary with Western Sahara turns from east to north. The intrusion has no visible morphological expression and is primarily delineated on satellite imagery. Limited outcrop suggests the presence of alternating bands of coarse to fine crystalline and fluidal textured syenite alternating with pink

granite of the Adam Esseder Complex, which it intrudes. The coarse crystalline syenite is a white to gray quartz-bearing rock with centimeter-scale amphiboles that takes on a pegmatitic appearance as crystal size increases. The amphiboles float in a matrix composed of feldspar and (rare) quartz. Minor local accumulations of fine crystalline green pyroxene are also present. Thin section work identifies the amphibole as arfvedsonite and magnetite, apatite, sphene, and rare biotite and epidote are present as accessory minerals. Fine-grained syenite has a mineralogical composition identical to the coarse crystalline variety and is distinguished from the pink granites of the Adam Esseder Complex by its high amphibole content and fluidal texture (Lahondère and others, 2003).

Based on geophysics and high scintillometer readings, two additional anomalies were located by the BRGM at El Mrhader in the northeastern quadrant of the Bir Moghreïn 1:200,000 scale geologic map and at El Hajar near the west edge of the Bel Guerdan 1:200,000 scale geologic map. Both anomalies have indications of potential for incompatible element deposits (Marot and others, 2003). El Mrhader is described as a magnetic and radiometric anomaly (K, Th, U) associated with a locally agpaitic granite with aplites and pegmatites. It is located about 25 km east-southeast of the Tabatanant occurrence in an area of voluminous granites and granodiorites of the Adam Esseder Complex. The El Hajar anomaly is located about 60 km east-southeast of the Tabatanant occurrence and also is in an area mapped as the Adam Esseder Complex. El Hajar is a non-outcropping magnetic and radiometric anomaly (U) that is associated with an aplite phase in regolith containing quartz and hematite and producing high scintillometer readings (400 c/s; Marot and others, 2003). Little else is known about these two locations.

Examination of the 1:200,000 scale geologic maps in the area of both the El Mrhader and El Hajar anomalies indicates that the igneous facies of the Adam Esseder that is present is the Bir En Nar monzogranite. It is described as a pink-colored, fine to coarse crystalline, rarely porphyritic rock with minor biotite. The rock is commonly highly potassic (up to 6 percent K_2O) and therefore trends towards syenogranitic compositions. Although commonly present as the dominant igneous rock over large areas, it also occurs as dikes and late-crystallizing “injections” into other phases of the Adam Esseder Complex. It thus bears some resemblance to the syenites and alkaline granites of the Tigsmat el Khadra Suite (Lahondère and others, 2003). Based on the presence of late crystallizing phases and the possible association with the Tigsmat el Khadra Suite, the El Mrhader and El Hajar anomalies are considered as permissive for the development of incompatible element concentrations. However, without additional field relationships and geochemical evaluation the potential for economic occurrences of REEs and incompatible elements must be regarded as unknown.

During the PRISM-I field campaigns carried out by the BRGM in the Paleoproterozoic portion of the Rgueïbat Shield, over 12,000 geochemical samples primarily consisting of gridded regolith samples and a lesser number of rock samples over specific features were collected and analyzed for multi-element geochemistry. The results of these analyses were processed by the USGS during the PRISM-II program and are presented in Eppinger and others (2015). In order to display single element data for such a large dataset containing several different types of sample media in a manner that draws attention to anomalously high geochemical results, Eppinger and others (2015) chose to display the data in terms of standard deviation (STD) units above the mean value

for the entire dataset of a given element. Five levels are displayed; <1.50, 1.51–2.00, 2.01–2.50, 2.51–3.00, and >3.00 STD. Examination of the data in ArcGIS format shows that targeted sampling programs were performed at the Tabatanat and Tigsmat occurrences and over the Bir Lefjah and Hassi El Fogra intrusions. A single rock sample was collected at the Assif Msérif intrusion. No sampling was performed at the Gara El Hamouïed and Bir Moghrein occurrences.

The Tabatanat occurrence has single element enrichments in multiple samples that are greater than 2.5 STD for K, Na, Sr, Ag, Nb, Ta, La, and Zr, and between 1.5 and 2.5 for Be, Cs, Ga, and Hf. These results do not support the presence of economic concentrations of REEs, however there may be potential for Nb-Ta. U and Th contents are not significantly above background concentrations. The Tigsmat occurrence has single element enrichments in several rock samples and in a suite of regolith samples collected from a series of dry streambeds draining the area to the southwest of the occurrence. Single element enrichments that are greater than 2.5 STD at Tigsmat include Ge, Hf, Nb, Rb, Y, Zr, and W, and between 1.5 and 2.5 for K, Na, Ga, Li, and Ta. As at Tabatant, these results do not support the presence of economic concentrations of REEs, however there may be potential for Nb-Ta. U and Th contents are not significantly above background concentrations.

BRGM sampling at the Hassi El Fogra syenite did not identify any elemental concentrations above 3 STD and only Ce, La, and Pr are at concentrations between 1.5 and 2.5 STD. This indicates low potential for REEs and that the intrusion is somewhat preferentially enriched in light REEs. The Bir Lefjah phonolite body is geochemically characterized by an extensive suite of single element enrichment above 3 STD for Al, Be, Ce, Co, Cu, Fe, Ga, K, La, Li, Mg, Mn, Na, Nb, P, Rb, Sr, Ta, W, Y, and Zn and STD between 1.5 and 2.5 for Cd, Cs, Eu, Ge, Sn, Te, Ti, U, and Zr. While potential for REEs is not indicated by the data, enrichments in base metals and a suite of elements often associated with hydrothermal alteration suggests that emplacement of the phonolite may have been associated with polymetallic vein or skarn mineralization. Potential for refractory metals may also exist.

Only one rock sample was collected by the BRGM from the Assif Msérif aegirine granite intrusion located to the southeast of the Tigsmat occurrence. This sample is characterized by single element enrichments greater than 3 STD of Be, Ga, Ge, Hf, Ho, Lu, Nb, Pb, Rb, Sn, Ta, Tb, Th, Tm, U, Y, Yb, Zr, and enrichments between 1.5 and 2.5 of Bi, and Gd. Significantly, this sample shows a clear enrichment in the more economically desirable heavy REEs as well as potential for U, Th, Nb, and Ta. Any future geochemical sampling in the region should include targeted sampling over the Assif Msérif intrusion in order to evaluate this very interesting geochemical anomaly.

4.3 Bou Naga Alkaline Complex

The Bou Naga alkaline complex contains most significant deposit of Y, Th, Ba, REEs and fluorite in Mauritania and has been the subject of numerous previous studies (see below). Here, the description presented is condensed slightly from the BGS report (see Gunn and others, 2004 and references therein).

The Bou Naga alkaline complex is a volcano-plutonic complex emplaced within the southeastern part of the Bou Naga tectonic window of Archean basement (Amsaga Complex; fig. 3). The magmatic complex broadly consists of a circular central multiphase

intrusion consisting of rocks of the Bou Naga Suite surrounded by ignimbritic outflow facies dominated by rhyolites, rhyodacites and trachytes of the Oued Tidoumaline Formation.

Two magmatic evolutionary series have been recognized within the Bou Naga Suite on the basis of geochemical and petrographic features: an early saturated suite that includes syenites, quartz syenites, alkali-feldspar granites and rhyolites followed by a subsaturated suite consisting of foid syenites to monzosyenites and phonolites. The intrusive massif is sub-circular with a diameter of about 12 km and is mainly composed of quartz syenites and alkaline granites (Trompette, 1963 and Marcelin, 1965). These quartz-bearing (saturated to oversaturated) alkaline rocks form a partial ring of hills with internal drainage into a central salt lake depression (sabkha). A later intrusive mass of foid-bearing undersaturated syenites and related hypabyssal intrusive rocks was emplaced into the south-central part of the complex and probably underlies part of the central depression (Blanc and others, 1985 and 1986; Blanc, 1986). The southern margin of the foid syenite exhibits an irregular tectonic contact with southward-dipping stromatolitic metalimestones of the para-autochthon (Nouatil Group; fig. 5). Three U-Pb zircon age measurements have been made on the alkaline complex. The syenite and alkaline granite are 676±8 Ma and 687±5 Ma, respectively (Blanc and others, 1992). A lower intercept of discordia on concordia of the host Archean orthogneiss also shows an age of 756±25 Ma linked with the emplacement of the alkaline complex (Blanc, 1986; Blanc and others, 1992).

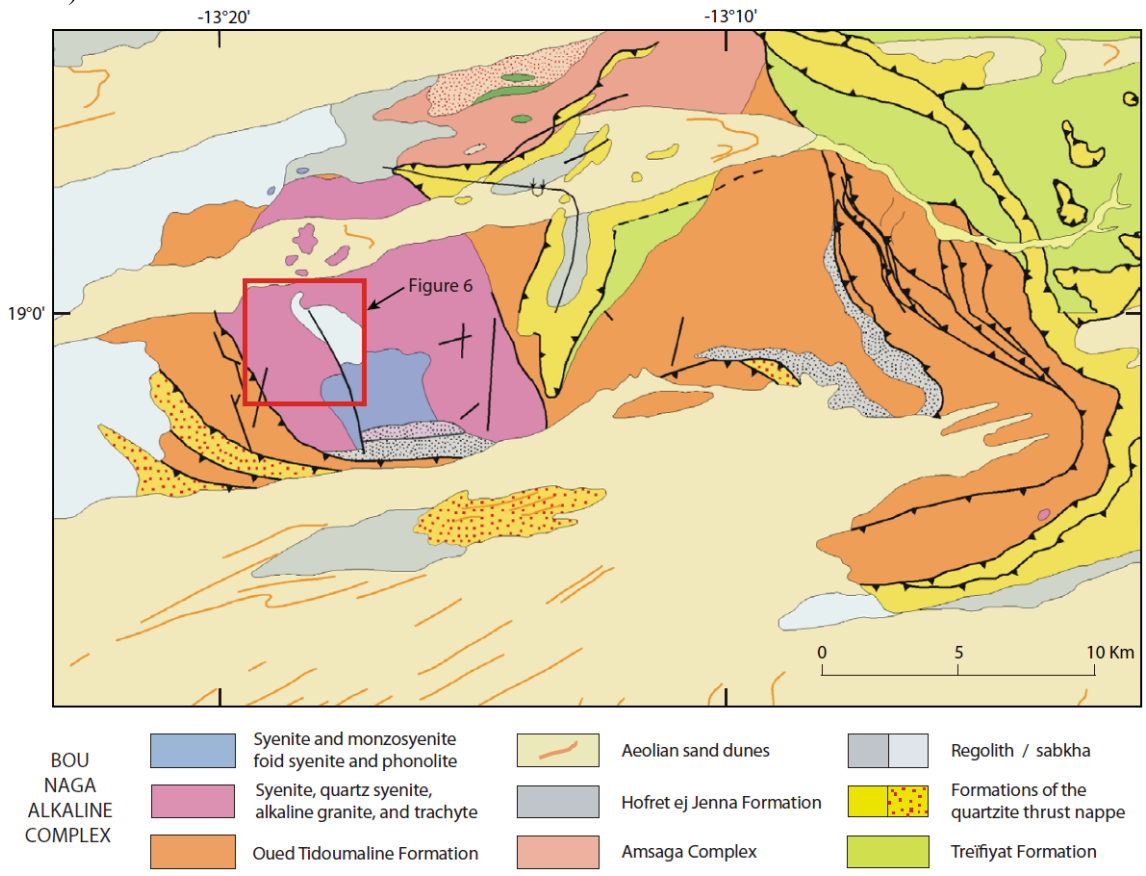

Figure 5. Geology of the Bou Naga Alkaline Volcano-Plutonic Complex (after Gunn and others, 2004).

The Oued Tidoumaline Formation and alkaline intrusive center consist of a caldera, ring-dike, and shallow pluton complex. The swarm of closely spaced rhyolitic dikes in the southwestern part of the intrusive complex may be the exposed root of a ring fissure. The Oued Tidoumaline Formation consists of the outflow sheets and peripheral pyroclastic deposits of the rhyodacitic volcano. These volcanics vary in composition from intermediate to peralkaline silicic and consist of proximal tuff breccias, ignimbritic flows and air-fall tuffs (Pitfield and others, 2004). The foid syenites of the undersaturated suite post-date the saturated (to oversaturated) syenite-alkali granite-rhyolite. Blanc and others (1986) consider that the foid syenite/monzosyenite suite is largely preserved in a central NNW-SSE-trending graben. This would be consistent with a laccolithic intrusion injected at shallow depth with a feeder conduit along the ring dike margin.

The Bou Naga alkaline complex, in common with other worldwide occurrences of alkaline igneous rocks, was emplaced in a continental rift or graben environment characterized by extensional tectonics and crustal thinning. Blanc and others (1986) consider that this autochthonous early Pan-African intrusive complex was emplaced during an anorogenic phase of intracontinental rifting which was initiated at 756±25 Ma.

The alkaline rhyolites occur as subvertical dikes and sheets in the southern part of the intrusive complex as well as in the eastern massif. They appear to be most abundant and well developed in the mine area to the west of the foid syenite mass where the rhyolites are cut and locally displaced by the more easterly-trending REE-Y-Th-F-Ba mineralized fault/fracture and vein sets.

The phonolites occur as narrow subvertical dikes (<2 m) and plugs within the coarse syenites. The dike orientation is most commonly WNW-ESE with a subsidiary NE-SW set. The dikes locally contain hematite shears/veinlets that parallel the dike margins while the plugs contain vuggy deposition of hematite and carbonate. The evidence suggests close spatial and temporal relationship with the mineralization.

Fracture-controlled quartz-hematite±fluorite±carbonate mineralization is widespread throughout the saturated suite of syenites, alkali granites and rhyolites of the Bou Naga Suite and parts of the surrounding Oued Tidoumaline Formation. Sub-economic REE-Y-Th-F-Ba vein mineralization occurs on the west side of the foid syenite intrusion and cuts both the saturated and undersaturated suites. This mineralization was the focus of several prospection campaigns by the Société Péchiney and was exploited briefly for yttrium and thorium by Société Somirema in 1967–1968 when an estimated 1,200 tonnes of yttrium concentrate was produced (Mining Annual Review, 1968–1970). The open cast workings dating from this period are largely filled with blown sand and are no longer accessible (fig. 6).

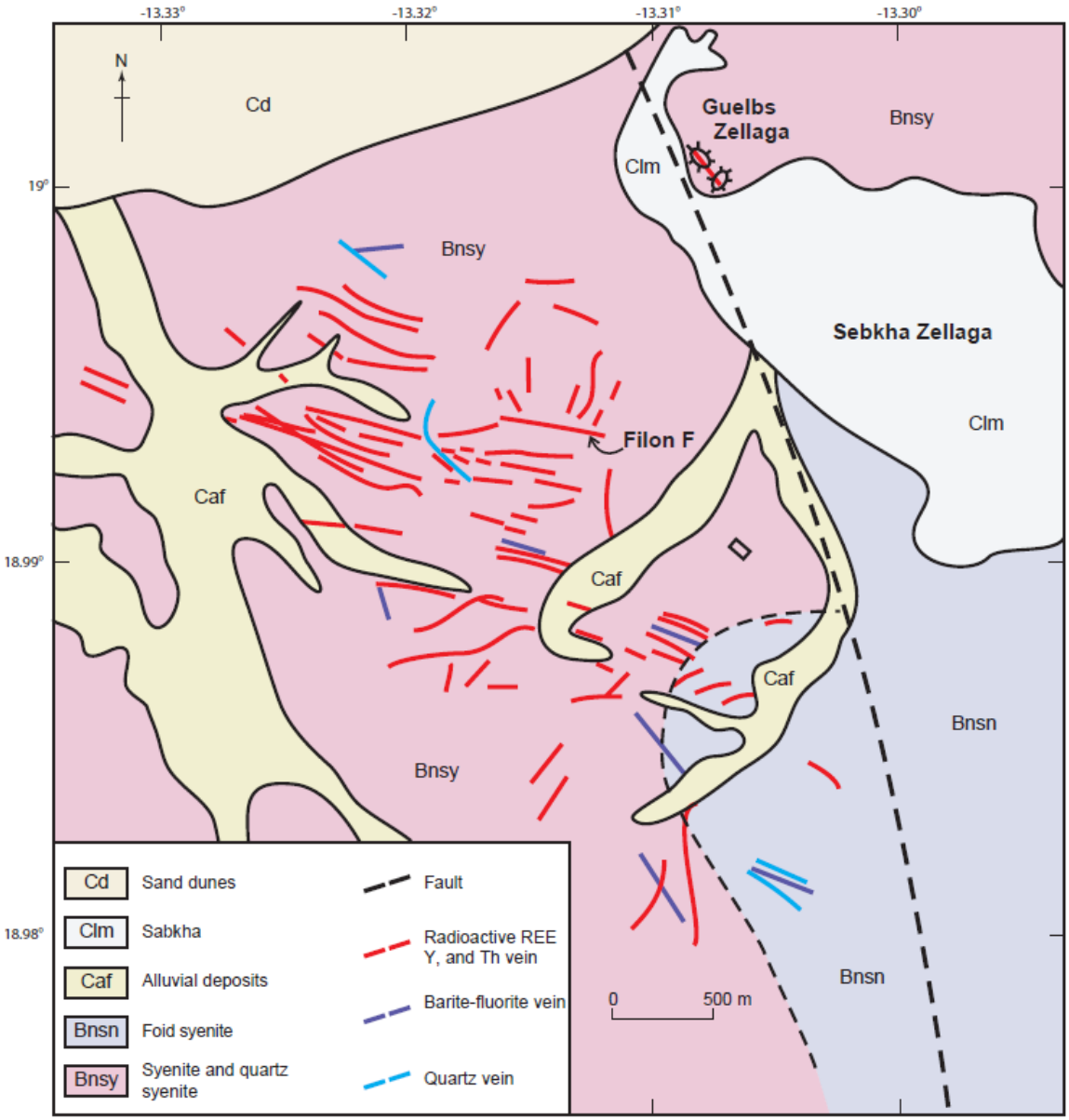

Figure 6. Plan of the mineralized veins in the area of the abandoned mine (plant site indicated by rectangle) in the south-west of Sebkha Zellaga (modified after Marcellin, 1965; Gunn and others, 2004). Location shown on figure 5.

The quartz-hematite shears and fracture-controlled veinlets/stringer zones have two dominant directions: NNW-SSE to NW-SE and E-W to WNW-ESE with subordinate sets trending ENE-WSW and N-S. They vary from tight anastomosing swarms to sparse shear/fracture coatings with a 1–10 meter spacing. The dense swarms have given rise to a general blackened appearance to some of the hills. The veins are up to 10 cm thick (most commonly <1–5 cm) and are locally banded or composite in type. In the mine area veinlets commonly carry small patches or lenticles of deep violet fluorite and exhibit centimeter-scale reddened wallrock alteration zones. This alteration extends up to 5 cm (mostly 2–3 cm) on either side of a <1 centimeter veinlet and reportedly up to a meter adjacent to meter-scale mineralized veins (Marcelin, 1965). The northwesterly shear-vein

sets exhibit sygmoidal geometry in relation to the EW-trending sets. Dilation of extensional link veins, offsets of rhyolitic dikes and other kinematic evidence indicate an apparent dextral component of lateral movement. Hematitic shears and fractures have a close spatial and temporal association with the vein mineralization in the mine area. They are observed in the footwall zone of the EW-trending mineralized veins.

Ten anomalous radiometric zones were defined within the Bou Naga volcano-plutonic complex during an aerogeophysical survey carried out by 'Compagnie Générale de Géophysique' of France in 1963–1964 (Marcelin, 1965). They correspond to zones where the airborne radioactivity measurements have exceeded 1,000 total counts per second. Four of these anomalies occur in the intrusive ring complex, three in the eastern rhyolitic massif and three within the volcanic suite of the Oued Tidoumaline tectonized block. In 1979 a second airborne geophysical survey organized by the UNDP was carried by Geoterrex Ltd. of Canada and identified an additional anomaly in this sector.

The principal site of former economic vein mineralization extends over an area of about 4 square km (km^2) and is hosted mainly by the saturated intrusive suite on the western side of the south-central foid syenite intrusion. A network of 62 veins have been recorded consisting of a dominant NW–SE to E–W trending swarm (average 110–120^o) and subordinate N–S to NE–SW sets (Marcelin, 1965). The veins are vertical or dip steeply northward and vary from a few tens of meters up to 1,500 m (Filon F) in length and from 2 cm to 5 m (average 30 cm) in thickness. The veining appears to terminate, or be truncated, to the east against a NNW-trending fault that passes through (or close to) the Guelbs Zellaga prospect (fig. 6).

The main vein swarm is hosted by shear-fractures and exhibits a degree of symmetry about the more easterly-trending set dominated by the Filon F fault reef. To the south of this axial trend the veins bend from a NW–SE orientation into parallelism with the fault reef whereas to the north they exhibit a curvature into a north-westerly trend. Filon F appears to have a left-stepping en echelon propagation and obliquely intersects some of the WNW–ESE veins. It constitutes the southern limit of a northerly set of veins and is itself cut by later quartz veins. The NNE–SSW veins are shorter and lenticular in form but attain greater widths. They are considered to be tensional fracture fillings.

Three types of veins are present: (1) radioactive veins that carry the REE, Y and Th minerals and have a dominant WNW-ESE trend, (2) barite-fluorite veins which parallel the radioactive veins but appear later in the vein paragenesis; barite and quartz are seen to cement and infill fragmented colloform hematite, and (3) quartz veins that trend NNE (030°) or NW–SE (130°) and both cut and displace the radioactive veins. They also postdate the barite-fluorite veins.

The radioactive shear-fracture veins (1 above) vary greatly in thickness and style of occurrence along strike. They commonly pinch and swell and (or) occur as intermittent lenses. Individual veins bifurcate and merge, pass into anastomosing stringer zones or ramifying networks and disseminations. The dilatational vein filling of the lower strain (?) sectors rarely exhibits regular banding and is mostly massive and brownish with a black patina. The internal structure of the veins is generally brecciated. Composite veins with two generations of quartz are present: early gray quartz-filled breccia veins are cut by pale milky quartz veins. The syenitic wallrocks and breccia fragments are commonly reddened by iron oxides.

Essential vein minerals include quartz, magnetite, hematite, goethite, cryptomelane, various carbonates, fluorite, rutile, thorite, pyrrhotite, pyrite, zircon, microcline and plagioclase. This assemblage may be accompanied locally by riebeckite ($Na_2Fe_5(Si_8)_{22}$), parisite ($CaCe_2(CO_3)_3$), bastnaesite ($LaCe(CO_3)(OH,F)$ and locally metamict xenotime (YPO_4). Thorium values commonly range from 0.1 to 6.5 percent and locally reach 12.5 percent in Filon F where the radioactive count locally peaks at 5,500 c/s and Y_2O_3 contents are 3.0–4.8 percent (Marcelin, 1965; Pouit, 1968). Thorianite (ThO_2), uranothorite $(U,Th,Ce)SiO_4$ and ilmenorutile $(Fe,Ti)O_2$ were additionally found in Filon F (Pouit, 1968).

Mineral resource estimates are stated as 1,850 tonnes per meter depth at an average grade of 3.65 percent Y_2O_3. Based on a workable depth of 40 m the total resource in place would be 74,000 tonnes of ore. However, in the absence of borehole intersections these estimates lack precision (Gunn and others, 2004).

The Guelbs Zellaga prospect (19°00'00"N., 13°18'25"W.; fig. 6) consists of quartz-carbonate-hematite-fluorite-barite-REE-mineralized alkali granite that forms a pair of conspicuous black jagged hills with a NW–SE oriented central spine. This prospect yields a strong uraniferous radiometric anomaly with U values mostly in the range 10–20.ppm U. Thorium values vary between 0.1 and 0.8 percent Th. The prospect is relatively enriched in cerium (bastnaesite) and is further distinguished by occurrences of malachite and epidote. Mineralization takes the form of a complex of veins, impregnation and replacement zones. In detail, this is resolved into approximately NW to NNW-trending vertical mineralized faults/veins and coalescing shallow SW-dipping fracture-controlled impregnation zones (flats). The mineralized faults and veins dip at 70–90°. A minor fault at 19°00'05"N. and 13°18'29"W. contains remnant vein boxworks outlining weathered-out breccia fragments and calcite-cemented debris. The northwest guelb (19°00'07"N., 13°00'29"W.) is characterized by conspicuous deep violet fluorite mineralization and rises to 45 m above the surrounding plain with a rectilinear western margin. The SE guelb (18°59'56"N., 13°18'25"W.) rises to 20 m, is more equidimensional and has a thick manganiferous ferricrete/gossan capping. Narrow quartz-breccia veins and vuggy cavities lined with quartz and calcite are evident within the massive hematite-goethite.

Overall the Guelbs Zellaga mineralization consists of a lens 330 m long and 85 m wide. Surface sampling on a systematic 10 meter grid (total of 153 samples) yielded Y_2O_3 values generally less than 0.2 percent, but with a mean grade for 100 samples of 2.5 percent CeO_2. An estimated 600,000 tonnes are readily exploitable without surface stripping.

Given the overall NW–SE trend, which is also apparent in the extensional vein and breccia systems near the margin of the ring complex and in the volcanic envelope, the mineralized system is interpreted as an extensional duplex or en echelon series of fractures. A dextral component of movement along a NW–SE fault zone would induce dilation in more northerly-trending fractures.

Epithermal veins and breccias cut the Oued Tidoumaline Formation and locally contain minerals of economic interest. In the eastern rhyolitic massif and Oued Tidoumaline block the quartz veins that trend NNE–SSW to NE–SW (030–036°), are typically 1–3 m thick and have a lateral extension of at least 200 m. The veins mostly consist of pale milky quartz but also locally contain clear and pale amethyst quartz.

Copper mineralization is evident from the showings of malachite, cuprite and a sooty black mineral, possibly chalcocite. Open-space filling textures (symmetrical colloform banding, comb textures and crystal-lined drusy cavities) are commonplace. Many veins also exhibit internal centimeter- to decimeter-scale zones of iron oxide-cemented brecciated vein quartz.

A suite of quartz-carbonate±sulfide veins trending WNW–ESE (280–305^{o}) cut the rhyodacitic volcanics of the eastern massif and chloritic schists of the Trefiyat Formation. They are typically anastomosing and lenticular in form (<40 cm thick) with a southward dip (47–72^{o}). Some examples are symmetrically banded with outer ankeritic margins to a coarsely crystalline white calcite zone containing a central seam with quartz lenses and well-formed pyrite cubes. The ankeritic layers also locally contain disseminated pyrite. Decameter-scale breccia zones/reefs trend WNW–ESE to NW–SE (300–316^{o}). Two types were identified: (1) quartz-cemented and silicified rhyolitic breccias containing small drusy cavities with quartz terminations (for example, 19°01'09"N., 13°21'14"W.), and (2) hematite±fluorite-cemented rhyolitic breccias exhibiting selective replacement and open space filling. (for example, 18°59'32"N., 13°09'00"W.). In some cases preferential impregnation of original volcanic breccias may have taken place.

It is evident that the vein mineralization has a close spatial, temporal and genetic association with the undersaturated suite of alkaline rocks. The late magmatic fluorine-rich residual fluids carrying high levels of incompatible elements (Ba, REE, Y, U, Th) have concentrated in dilational (extensional) sites of fault/fracture zones. The presence of LREE fluorocarbonates further indicates that CO_2 was a significant component of the pneumatolitic fluid phase.

The first stage of mineralization generated the hematitic vein swarms, the radioactive REE-bearing and fluorite-barite veins. The paragenesis is condensed or telescoped but in general indicates early deposition of Fe, Mn, REE and Y minerals and later deposition of Ba, F and U minerals. The silicates were deposited early and are closely associated with U. Quartz and to a lesser extent fluorite can occur throughout; calcite becomes increasingly common towards the end stages of deposition. U and Th would preferentially partition into a gaseous phase with wider dispersion that may partly explain the widespread radiometric anomalies.

The second stage of mineralization was associated with compressional (or transpressional) nappe tectonics with the introduction of quartz veins and some remobilization of the pre-existing mineralized veins, particularly Th and U. Other minerals associated with this mineralization include hematite, carbonates, Cu minerals and other sulfides, principally pyrite. Ankerite borders the WNW–ESE trending veins in the eastern massif and clearly predates the other mineral phases.

Centimeter-scale drag folds and other unspecified kinematic indicators indicate a sinistral component of lateral movement on Filon F (Blanc, 1986). This would be consistent with the sense of curvature/rotation of the veins into Filon F fault zone. However, the en echelon array is wrongly cited as evidence for this movement vector; the geometry is not diagnostic. Left-stepping en echelon fractures in a simple strike-slip system with a sinistral movement sense would be fundamentally anti-dilational (R1 synthetic shears). Dilational fissure fillings are considered to be: (1) in response to a significant normal (extensional) component to the fault movement, (2) largely due to hydraulic brecciation in a compressional environment. E-W to NE-SW inflexions to the

WNW-trending lodes would dilate in an essentially compressional environment and may have acted as loci for the brecciation, or (3) early extensional phase of fissure filling was supplanted by an essentially compressional regime.

Dextral offsets of some NW-SE rhyolite and microsyenite dikes are observed along minor faults paralleling the approximate EW-trending vein system. Extensional link veins between EW-trending shear veins also imply a dextral component of movement. Contra-indications of movement sense on the EW to WNW structures would tend to favor a shear sense reversal.

The NNW–SSE trending Guelbs Zellaga mineralization has been emplaced along a subvertical fault zone. Late faulting and subparallel quartz veining have a dextral component of movement. Some northwesterly-trending hematite stringer/fracture zones also have a dextral shear sense. Mineralization extends along subhorizontal fractures in the form of impregnation zones or flats. Extensional flat-lying to shallow-dipping reefs of little lateral persistence are typically generated within a compressional environment. Intuitively fundamentally dilational sites (extensional jogs) are especially favorable for hydrothermal mineralization.

In relation to a strain ellipsoid the Guelbs Zellaga and Filon F fault systems may have initiated as Riedel shears, or in the case of the Filon F swarm tensional structures (veins or normal faults) in response to a NW-SE-directed far-field stress. As Reidel shears the Guelbs Zellaga and Filon F fault zones would have a sinistral and dextral components of movement respectively. This stress regime would favor the formation of extensional flat-lying mineralized structures within the acute bisectrix of these faults. Later reorientation of the stress field to a north-easterly compressional azimuth would reactivate these structures in the opposite sense. Sinistral movement along the Filon F system could explain the sygmoidal nature of the vein system, the obliquely intersecting synthetic shears and initiation of late NE- to NNE-trending quartz veins (R1 shears or tensional fissures). The extensional environment during the main phase of mineralization would be associated with the closing stages of the rift phase, which permitted the injection of the alkaline magmas at 680±10 Ma. The reorientation of the stress field would have coincided with the Pan-African orogeny, which commenced at about 650 Ma and continued until a continent-continent collisional event during the period 620–580 Ma (Dallmeyer and Lécorché, 1989).

4.4 Carbonatites

The only known occurrence of carbonatite in Mauritania is within the Richat structure located in the northwest Taoudeni Basin. Van Alstine and Schruben (1980) report three carbonatite occurrences in the Anerat Eizaughe area but these have not been confirmed.

4.4.1 Guelb er Richat

The Richat Structure is one of the most famous of terrestrial features as seen from space and because of its appearance from above is sometimes called "The Eye of Africa" (Matton and Jébrak, 2008). It consists of a slightly elliptical annular structure approximately 45 km in diameter (fig. 7). It had been proposed as an impact structure but subsequent work has not supported this interpretation and it is now viewed as a structural dome above an igneous intrusive complex (Fudali, 1969, Dietz and others, 1969; Matton

and others, 2005). The structure consists of an outer zone of Neoproterozoic to Ordovician sedimentary rocks that dip outwards with a maximum dip of 20–25 degrees near the center of the structure, which decrease in dip outwards. The inner or core zone is approximately 6 km in diameter and consists of a complex of limestone, clastic sedimentary rocks, breccia and altered volcanic rocks (Dietz and others, 1969; Woolley and others, 1984; Matton and others, 2005). Fieldwork in 2007 by a USGS team permitted field observation and sampling of many of the rock units described. Results of multielement geochemical analyses of carbonatite dikes, basaltic dikes, sedimentary rocks, and silicified breccias are presented in table 1A. Descriptions of samples are presented in table 1B.

Dietz and others (1969) mention the presence of a smaller and less well exposed circular structure of similar character as Guelb er Richat at Semsiyat located 50 km to the west southwest (fig. 7). Although no carbonatite dikes or other intrusive rocks are known at Semsiyat mainly due to lack of outcrop, there are float fragments of chert breccias at its center, similar to breccias at the center of Guelb er Richat (Dietz and others, 1969).

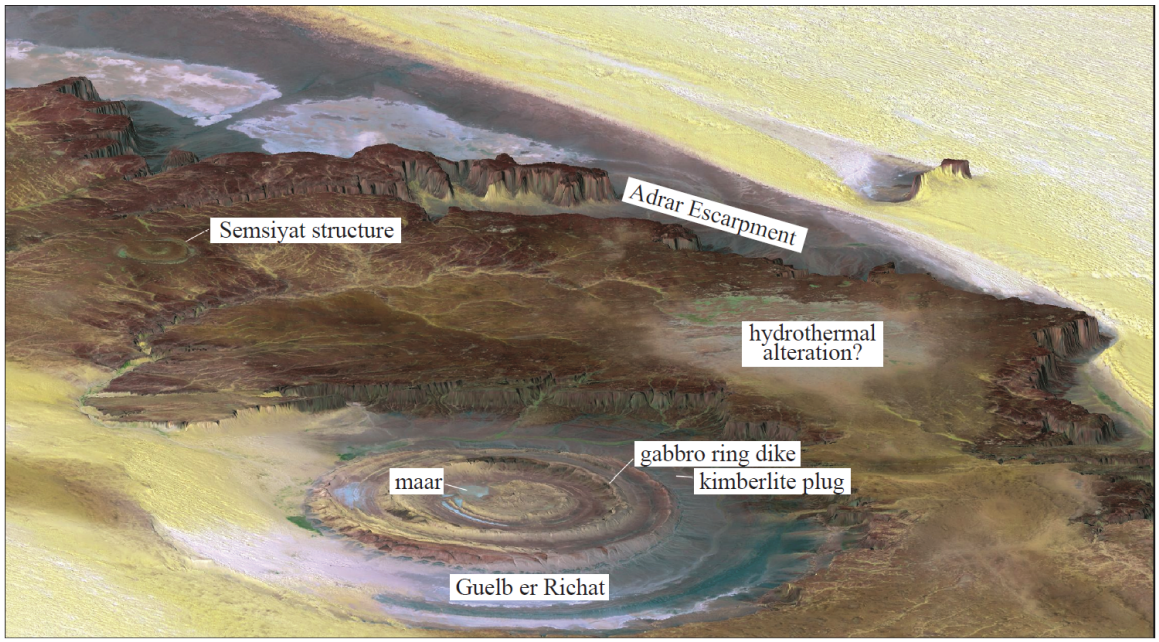

Figure 7. Landsat TM RGB composite satellite image draped on a SRTM Digital elevation model of the Geulb er Richat structure viewed obliquely from the northeast (6x vertical exaggeration). Note smaller Semsiyat dome to the southwest. Image from NASA (http://photojournal.jpl.nasa.gov/catalog/PIA04963).

Four types of igneous rocks are known to occur within or near the Richat structure: gabbro dikes, carbonatite dikes, a kimberlite plug and associated sills, and extrusive rhyolite (Matton and Jébrak, 2008). The gabbro and carbonatite dikes intrude the outer zone, the rhyolite occurs within the core zone, and the kimberlite lies outside the dome near its northwestern margin (figs. 7 and 8).

The gabbros occur as two ring dikes within the structure at distances of approximately 3 and 7 to 8 km from the center of the dome and are approximately 20 and

50 m wide, respectively (fig. 8). They are medium to fine-grained and have a primary assemblage of mainly plagioclase and clinopyroxene with minor amphibole, biotite, and magnetite (Matton and Jébrak, 2008). They are partially altered to secondary amphibole and chlorite. Chemically, the gabbros are quartz and hypersthene normative and have normative plagioclase compositions of An57-62 and FeOt>MgO (table 2). They are not alkaline but rather have continental tholeiite chemistry. The gabbroic rocks have not been dated.

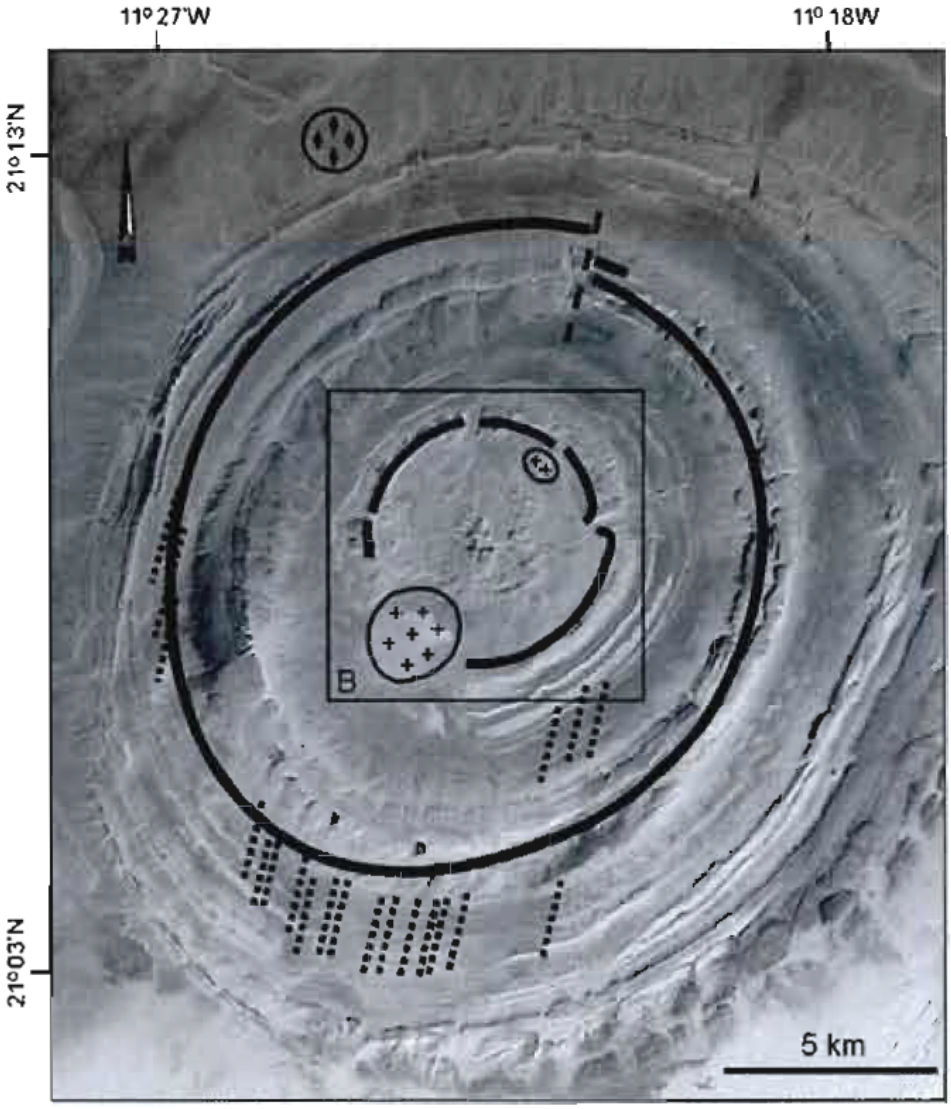

Figure 8. Geologic features of the Guelb er Richat structure overlain on satellite imagery from Matton and Jébrak (2008) (black heavy lines = gabbroic ring dikes; crosses = rhyolitic volcanic craters; diamonds = kimberlite plug and sill, dotted lines = carbonatite dikes; and dashed line = fault). Note: square box labelled B refers to another map figure in the Matton and Jébrak (2008) paper.

Although the presence of dike-like carbonate bodies within the structure had previously been observed, Woolley and others (1984) definitively identified these as carbonatites. Woolley and others (1984) identified dikes in the southern part of the

complex and Blanc and Pomerol (1973) reported the common presence of carbonatite dikes in the Tin Jouker area in the northwest portion of the dome. Matton (2008) has mapped thirty-two carbonatites dikes and a few sills from the southern and western parts of the structure (fig. 8). All occur in the outer zone of the structure and some intrude the outer gabbro ring dike (Matton and Jébrak, 2008). They are 1–4 m wide and up to 300 m long (Matton and Jébrak, 2008; fig. 9*A–C*). PRISM-I studies indicate the area of the carbonatite dikes at Guelb er Richat to be coincident with a high thorium geophysical anomaly (O'Connor and others, 2005). Although Woolley and others (1984) interpreted the dikes to have a radial geometry from the center of the structure this is refuted by Matton and Jébrak (2008) who indicate they occupy a fracture system oriented at N15-20ºE (fig. 8).

A. 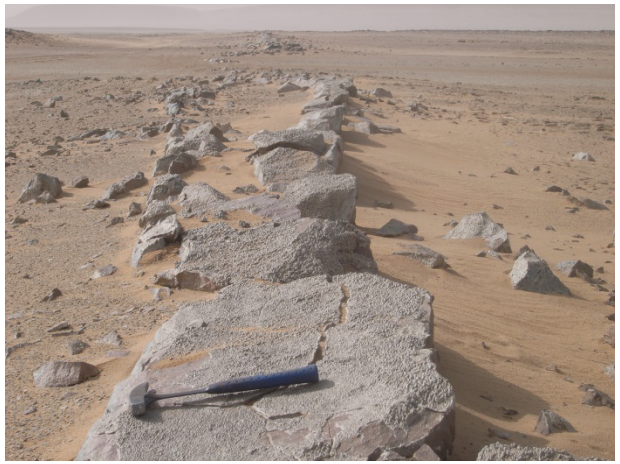

B. 

C. 

D. 

Figure 9. Photos of carbonatite dikes and breccias in the Geulb er Richat structure: *A*, 1–2 meter thick carbonatite dike; *B*, bifurcation in carbonatite dike; *C*, close-up showing texture of carbonatite; *D*, close-up of silicified breccia showing jasper and other sedimentary rock clasts floating in silicified matrix. USGS photos.

The grain size of the carbonatite is fine- to medium-grained. Texture is variable being locally porphyritic with a fine-grained groundmass. A banded fluidal structure in many of the dikes suggests multiple magma injections (Matton and Jébrak, 2008). Vugs and coarse carbonate veinlets are common. Various degrees of silicification are also observed. Xenoliths of chert and sandstone locally occur within the dikes.

Based on available whole-rock chemistry (tables 1 and 3) the carbonatites are all magnesiocarbonatites with a fairly narrow compositional range (fig. 10). Geochemical analyses of carbonatite indicate elevated concentrations of Nb, Sr, Ba, U, and Th close to average magnesio- and calciocarbonatites. Woolley and others (1984) noted P_2O_5 concentrations consistent with 4–5 percent modal apatite.

Table 1*A*. Selected USGS analytical results from ICP-AES-MS55 geochemistry of gabbroic dikes, carbonatite, siliceous breccias, and sedimentary rocks from Guelb er Richat. Major elements (Al, Fe, Mg, Ca, K, and P) in percent all others in parts per million (ppm). All field numbers in analytical results table have prefix of CT07RIM. See table 1*B* for sample description information.

Sample	42-1	46-1	41-1	43-1	46-2	45-1	41-2	44-1	44-2
Lithology	gabbro	micro-gabbro	carbonatite	carbonatite	silicified dolomite breccia	siliceous breccia	sandstone	dolomite	dolomite
Al	7.61	8	0.19	0.79	4.23	2.51	3.32	0.5	0.15
Fe	7.8	6.5	5.17	5.48	0.35	0.69	1.06	0.94	0.21
Mg	3.79	3.63	8.61	6	0.14	1.22	0.57	10.2	11.4
Ca	7	6.9	19.9	17.5	14.2	3.8	1.4	19.8	19.1
K	0.5	1	<0.1	<0.1	6.2	3.1	1.2	0.6	0.1
P	0.08	0.08	0.92	1.32	6.38	0.03	0.03	0.77	0.04
Ba	244	878	5180	3110	820	>10000	415	94.1	281
Be	<5	<5	<5	7	72	6	<5	7	<5
Ga	17	15	6	8	17	7	9	1	<1
Ge	2	2	1	2	2	2	1	1	<1
Hf	3	2	2	3	3	9	16	<1	<1
Ho	0.89	0.75	3.82	3.72	27.9	4.58	0.77	3.19	0.26
Li	20	20	<10	30	60	220	120	20	<10
Nb	8	10	536	1140	25	47	21	15	14
Rb	21.4	44.2	0.9	4.5	245	119	58.9	15.9	3.7
Sc	35	35	26	12	23	9	5	7	<5
Sr	195	242	1880	2960	1750	172	104	422	124
Ta	0.5	0.7	12.3	41.1	0.7	1.2	0.9	<0.5	0.6
Th	2.4	3.6	117	163	>1000	103	19.6	79.8	7.4
U	0.59	0.42	7.58	39.6	74	1.51	1.95	2.68	0.72
Y	22.1	18.4	86.2	84.9	708	114	21	79.2	7.4

Table 1*A*. Selected USGS analytical results from ICP-AES-MS55 geochemistry of gabbroic dikes, carbonatite, siliceous breccias, and sedimentary rocks from Guelb er Richat. Major elements (Al, Fe, Mg, Ca, K, and P) in percent all others in parts per million (ppm). All field numbers in analytical results table have prefix of CT07RIM. See table 1*B* for sample description information.—Continued

Sample	42-1	46-1	41-1	43-1	46-2	45-1	41-2	44-1	44-2
Lithology	gabbro	micro-gabbro	carbonatite	carbonatite	silicified dolomite breccia	siliceous breccia	sandstone	dolomite	dolomite
Zr	98.1	92.4	106	190	104	343	608	121	4.7
La	12.6	14.9	784	661	49.4	16.2	28	5.3	10.5
Ce	26.9	30.5	1370	1230	134	35.4	63.2	13.1	18.9
Pr	3.7	4.04	151	138	26.5	4.89	7.65	2.12	2.22
Nd	15	14.5	467	426	169	23.8	26.5	12.5	7.2
Sm	4.1	3.6	68.1	61.8	158	17.2	5.1	10.5	1.5
Eu	1.26	1.04	17.3	15.6	76.7	7.53	0.9	5.43	0.46
Gd	4.17	3.93	40.3	35.3	277	29.9	3.49	21	1.68
Tb	0.63	0.59	4.94	4.56	46.8	5.86	0.58	4.01	0.27
Dy	4.1	3.91	22.8	21.8	218	29.6	3.58	20.8	1.79
Er	2.42	2	8.47	8.29	49.1	9.73	2.24	6.47	0.66
Tm	0.35	0.3	0.96	1.03	4.77	1.17	0.36	0.75	0.07
Yb	2.2	1.8	5.3	5	21.9	6.5	2.6	3.8	0.4
Lu	0.36	0.29	0.75	0.6	2.52	0.94	0.43	0.48	0.1

Table 1*B*. Description of samples presented in table 1*A*.

Field No.	Unit name	Lithology	Sample Description
CT07RIM41-1		carbonatite	1-2m-thick carbonatite dike along piste into center of structure.
CT07RIM41-2	Assabet El Hassiane Gp-Abiodh Sub-Gp	sandstone	Thin-bedded reddish fine grained sandstone. Collected from immediately adjacent to the carbonatite dike at this location.
CT07RIM42-1	Mgd	gabbro	Coarse crystalline gabbro. 10m diameter outcrop of low relief.
CT07RIM43-1		carbonatite	0.7m thick phenocrystic carbonatite dike. Pervasive brick red weathering. Dike is either flow banded or is composite banded due to multiple injections of carbonatite.
CT07RIM44-1	Atar Gp-Tifounke Fm	dolomite	Outcrop of stromatolitic dolomite. Fractured sample with late dolomite cement.
CT07RIM44-2	Atar Gp-Tifounke Fm	dolomite	Outcrop of stromatolitic dolomite. Sample of dark gray non-porous flint-hard dolomite.
CT07RIM45-1	Atar Gp-Tifounke Fm	siliceous breccia	Outcrop of siliceous breccia. Light tan on fresh surfaces with clasts of red jaspar and black chert. 1200 cps scintillometer reading.
CT07RIM46-1	Mgd	microgabbro	Outcrop and subcrop of microgabbro in floor of inner sabkha-covered ring. Sample of freshest gabbro.
CT07RIM46-2	Atar Gp-Tifounke Fm	silicified dolomite breccia	Outcrop of silicified dolomite breccia 100m inward from gabbro outcrops. 1200 cps scintillometer reading.

Table 2. Richat structure gabbro analyses from Matton (2008). Major elements in weight percent oxides and trace elements in parts per million (ppm) (analytical method ICP-MS, lithium borate fusion).

Sample	44	57	143	144	116	122	136
SiO_2	51.33	51.28	52.21	51.72	51.24	50.80	51.71
TiO_2	1.06	1.27	1.00	1.00	1.10	1.22	0.86
Al_2O_3	15.27	15.25	14.49	14.56	15.00	14.30	14.33
FeO	9.50	10.32	9.29	9.46	9.98	10.83	9.45
MnO	0.18	0.20	0.15	0.16	0.17	0.18	0.16
MgO	6.91	6.42	7.42	7.55	6.26	6.88	7.59
CaO	10.00	9.70	10.09	10.45	10.32	10.23	10.62
K_2O	0.80	0.54	0.88	0.79	0.72	0.64	0.82
Na_2O	2.06	2.27	2.18	2.09	2.35	2.14	2.12
P_2O_5	0.17	0.15	0.18	0.15	0.11	0.14	0.18
Cr_2O_3	0.04	0.02	0.05	0.05	0.01	0.01	0.06
LOI	1.91	1.60	1.00	0.80	1.60	1.80	1.00
Total	**99.23**	**99.02**	**98.94**	**98.78**	**98.86**	**99.17**	**98.90**
CIPW cation normative minerals:							
%AN	61.9	59.4	58.1	59.9	57.3	58.9	58.8
Q	4.43	4.90	4.16	3.61	3.61	3.58	3.07
or	4.89	3.31	5.33	4.79	4.41	3.92	4.97
ab	19.13	21.12	20.07	19.24	21.87	19.93	19.52
an	31.09	30.92	27.85	28.73	29.28	28.56	27.87
di	15.26	14.36	17.83	18.75	18.43	18.52	19.98
hy	20.53	20.24	20.27	20.46	17.77	20.47	20.44
mt	2.77	3.00	2.68	2.68	2.82	2.95	2.53
il	1.53	1.83	1.43	1.43	1.59	1.76	1.23
ap	0.37	0.33	0.39	0.32	0.24	0.30	0.39
Co	40.8	45.7	42.2	41.8	45.1	45.1	46.1
Ni	77.8	83.3	17.2	16.7	60	40	20.8
V	242	285	238	226	293	324	274
As	3.8	5.8	1.3	0.8	2.7	3.4	18.8
Rb	26.2	17.8	28.2	24.5	23.1	22.5	26.5
Sr	234	235	246.8	212	248.6	230.4	263.2
Zr	73.1	32.1	95	93.2	5.1	94.2	80.2
Bi			0.3	0.3			
Sb	0.1	0.2	0.2	0.1			
Ga	15.5	18.7	16.4	16.3	18.1	18.3	10
Nb	14.5	8.1	9.3	9.3	11.2	9.7	16.1
Cd	0.1	0.1	0.2	0.1	0.1	0.1	

Table 2. Richat structure gabbro analyses from Matton (2008). Major elements in weight percent oxides and trace elements in parts per million (ppm) (analytical method ICP-MS, lithium borate fusion). —Continued

Sample	44	57	143	144	116	122	136
CIPW cation normative minerals:							
Cs	0.9	0.5	1.2	1.3	1	1	1.7
Ba	781	831	388.7	276.7	226.4	228.7	439.9
Hf	2.3	1.3	2.5	2.6	2.9	2.6	2.5
To	0.7	0.5	0.8	0.7	0.6	0.4	0.8
Pb	4.4	13.1	15.5	8.6	19	10.1	2
Zn	80.2	107.8	50	38	49	44	21
Ag	134	86	0.1				
Mo	0.8	0.4	1.5	0.8	0.3	0.5	0.4
Cu	89	48.8	88.8	88.8	126.8	127.7	83.8
Sn	1	0.9			1	1	1
W	0.8	0.8	0.8	0.4	0.5	0.4	0.2
Au			2.1	2.5	2.7	0.6	1.2
Th	3.7	2.7	3.4	2.8	2.4	2.5	3.7
Be	1	1	1	1	1	1	
Y	20.3	23	22.4	21.5	22.1	22.3	20.9
Sc	32.8	33.5	35	35	34	35	35
U	0.7	0.4	0.8	0.7	0.6	0.6	0.7
La	17	11	14.9	14.2	12.3	12	18
Ce	37.8	29.2	31.1	29	28	27.2	33.6
Pr	4.1	3.4	3.8	3.6	3.5	3.4	4
Nd	16.1	13.5	15.2	15.9	14.6	15 6	16
Sm	3.7	3.6	3.4	3.4	3.2	3.3	3.5
Eu	1.3	1.2	1.1	1.1	1.1	1.1	1
Gd	3.8	4.1	4	3.7	3.8	3.7	3.5
Tb	0.7	0.8	0.7	0.6	0.7	0.7	0.7
Dy	4.1	4.8	3.9	3.7	4	3.8	3.5
Ho	0.7	0.9	0.8	0.8	0.8	0.8	0.7
Er	2.8	2.8	2.4	2.3	2.3	2.3	2.1
Tm	0.3	0.3	0.4	0.4	0.3	0.3	0.3
Yb	2.4	2.4	2.2	2.1	2.1	2	1.8
Lu	0.3	0.3	0.3	0.3	0.3	0.3	0.3

%AN = an/(an + ab) * 100; the Ca/Ca+Na) ratio in normative plagioclase expressed in percent.

Table 3. Major and trace element chemistry of carbonatites from the Guelb er Richat structure. Samples 30 to 114 are from Matton (2008), P12 prefixed samples are from Woolley and others (1984) and samples 41-4 and 43-1 from Table 1*A*. Samples CC, MC, and FC are average carbonatites analyses from Woolley and Kempe (1989) (CC - calciocarbonatite, MC - magnesiocarbonatite, and FC - ferrocarbonatite).

Sample	30	35	110	111	114	P12--72	P12--73	P12--77	P12--78	41--4	43--1	CC	MC	FC
SiO_2	1.44	2.35	0.56	5.83	12.92	2.46	2.05	5.26	4.72	--	--	2.72	3.63	4.7
TiO_2	0.62	0.77	0.12	0.09	0.14	0.11	0.11	0.17	0.16	--	--	0.15	0.33	0.42
AI_2O_3	1.89	2.27	0.75	0.92	1.21	0.8	0.8	2	2	0.36	1.49	1.06	0.99	1.46
Fe_2O_3	--	--	--	--	--	0.2	0.09	0.04	0.05	--	--	2.25	2.41	7.44
FeO	8.55	7.44	7.32	8.18	7.39	6.72	6.69	6.46	6.49	6.65	7.05	1.01	3.93	5.28
MnO	0.7	0.55	0.68	0.81	0.8	1.19	1.2	0.4	0.5	--	--	0.52	0.96	1.65
MgO	12	12.52	14.82	13.85	11.66	13.7	14.9	13.34	13.84	14.28	9.95	1.8	15.06	6.05
CaO	25.49	25.41	30.46	27.28	26.15	30	29.05	28.69	28.66	27.84	24.49	49.12	30.12	32.77
Na_2O	0.34	0.38	0.31	0.18	0.39	0.24	0.23	0.44	0.44	--	--	0.29	0.29	0.39
K_2O	0.04	0.05	0.04	0.07	0.04	0.03	0.03	0.04	0.07	--	--	0.26	0.28	0.39
P_2O_5	1.41	1.12	3.09	0.85	3.33	2.21	2.04	3.07	2.32	2.11	3.02	2.1	1.9	1.97
Cr_2O_3	0.008	0.011	0.001	0.002	0.003	--	--	--	0.01	--	--	--	--	--
SO_3	--	--	--	--	--	1	0.7	0.7	0.4	--	--	0.88	1.08	4.14
BaO	0.05	0.1	0.02	0.96	0.7	0.89	0.97	0.2	0.12	0.58	0.35	0.34	0.64	3.25
SrO	0.38	0.17	0.38	0.25	0.61	0.42	0.38	0.37	0.35	0.22	0.35	0.86	0.69	0.88
F	--	--	--	--	--	0.13	0.14	0.11	0.11	--	--	0.29	0.31	0.45
CO_2	--	--	--	--	--	40	39.44	37.13	37.81	--	--	36.64	36.81	30.74
H_2O--	--	--	--	--	--	0.25	0.14	0.25	0.21	--	--	--	--	--
H_2O+	--	--	--	--	--	0.08	0.78	1.26	1.3	--	--	0.76	1.2	1.25
LOI	45.03	44.64	40.2	39.1	33.4	--	--	--	--	--	--	--	--	--
Totals	**97.51**	**97.51**	**98.14**	**97.14**	**87.39**	**100.43**	**99.74**	**99.93**	**99.56**	**--**	**--**	**101.05**	**100.63**	**103.23**

Table 3. Major and trace element chemistry of carbonatites from the Guelb er Richat structure. Samples 30 to 114 are from Matton (2008), P12 prefixed samples are from Woolley and others (1984) and samples 41-4 and 43-1 from Table 1*A*. Samples CC, MC, and FC are average carbonatites analyses from Woolley and Kempe (1989) (CC - calciocarbonatite, MC - magnesiocarbonatite, and FC - ferrocarbonatite).—Continued

Sample	30	35	110	111	114	P12--72	P12--73	P12--77	P12--78	41--4	43--1	CC	MC	FC
V	176	179	119	175	152	--	--	--	--	--	--	80	89	191
Sc	6.7	6.9	18	22	17	--	--	--	--	26	12	--	--	--
Co	11.4	15	7.7	4.1	7.1	--	--	--	--	--	--	11	17	26
Ni	17.6	64.1	12.5	11.3	7.7	--	--	--	--	--	--	18	33	26
Cd	0.3	0.3	0.2	0.1	0.3	--	--	--	--	--	--	--	--	--
As	32.2	31.2	4	11.4	22.2	--	--	--	--	--	--	--	--	--
Bi	0.2	0.2	785.4	306	0.1	--	--	--	--	--	--	--	--	--
Sb	0.6	0.5	0.4	0.2	0.3	--	--	--	--	--	--	--	--	--
Rb	1.7	3.4	1.4	2	1.4	--	--	--	--	--	--	14	31	--
Sr	3199	1475	3240.4	2134.9	5195.2	3551	3213	3129	2960	1880	2960	7272	5835	7441
Ba	479	864	205.6	8556.2	6271.6	7969	8685	1791	1074	5180	3110	3044	5730	7163
Ga	2.8	3.5	4.2	4.7	5.2	--	--	--	--	6	8	--	--	--
Ge	--	--	--	--	--	--	--	--	--	1	2	--	--	--
Nb	84.6	104	816.4	112.4	1598.1	800	815	340	245	536	1140	1204	569	1292
Ta	0.8	0.6	47.5	4.5	51.1	31.5	33.6	28.6	20.9	12.3	41.1	5	21	0.9
Be	1	1	1	2	3	--	--	--	--	<5	7	2.4	1	12
Li	--	--	--	--	--	--	--	--	--	<10	30	--	--	--
Cs	0.3	0.4	0.9	0.1	1.3	--	--	--	--	--	--	20	0.9	0.6
Cu	9	11.8	9	2.2	34	--	--	--	--	--	--	--	--	--
Pb	26.8	13.4	9.6	12.5	6.6	--	--	--	--	--	--	56	89	217
Zn	81.8	71.3	280	77	132	--	--	--	--	--	--	188	251	606
Ag	1034	645	--	--	0.2	--	--	--	--	--	--	--	--	--
Au	--	--	1.2	5.1	3.1	--	--	--	--	--	--	--	--	--
Mo	0.4	0.4	0.4	0.4	0.3	--	--	--	--	--	--	--	--	--
Sn	1.2	1.1	4	--	4	--	--	--	--	--	--	--	--	--
W	6.9	4.9	2.3	1.5	2.1	--	--	--	--	--	--	--	--	--

Table 3. Major and trace element chemistry of carbonatites from the Guelb er Richat structure. Samples 30 to 114 are from Matton (2008), P12 prefixed samples are from Woolley and others (1984) and samples 41-4 and 43-1 from Table 1A. Samples CC, MC, and FC are average carbonatites analyses from Woolley and Kempe (1989) (CC - calciocarbonatite, MC - magnesiocarbonatite, and FC - ferrocarbonatite).

Sample	30	35	110	111	114	P12--72	P12--73	P12--77	P12--78	41--4	43--1	CC	MC	FC
Y	75.8	42.2	79.5	84.3	147.7	75	85	35	40	86.2	84.9	119	61	204
Th	59.6	29.7	95.7	155.2	258.3	173	184	48	39	117	163	52	93	276
U	9	4.4	30.4	1.5	80.8	31.9	35.1	21.7	19.7	7.58	39.6	8.7	13	7.2
Hf	2.2	2.6	1.8	0.9	3.5	--	--	--	--	2	3	--	--	--
Zr	186.9	174.5	142.3	49.3	249.8	550	470	500	470	106	190	189	14	127
Rare-earth-elements:														
La	546	319	681.5	1157.2	872.8	1040	1125	284	330	784	661	608	764	2666
Ce	849.8	482.4	1254.1	1706.4	1681.1	2000	2140	610	680	1370	1230	1687	2183	5125
Pr	95.5	55.6	132.6	160	176.7	--	--	--	--	151	138	219	560	550
Nd	327.7	188.4	434.1	481.1	588.8	--	--	--	--	467	426	883	634	1618
Sm	44.2	26.4	59.6	55.7	72.4	590	610	222	241	68.1	61.8	130	45	128
Eu	11.8	7.2	15.8	13.9	20.2	19.4	20.3	8.66	9.3	17.3	15.6	39	12	34
Gd	25.3	15.8	31.9	30.7	45.9	--	--	--	--	40.3	35.3	105	--	130
Tb	4.2	2.4	4.4	4.6	7.8	8.04	8.04	3.34	3.36	4.94	4.56	9	4.5	16
Dy	18.4	10.3	18.8	20.7	33.6	--	--	--	--	22.8	21.8	34	--	52
Ho	3	1.6	2.9	3	5.1	--	--	--	--	3.82	3.72	6	--	6
Er	9.1	4.6	7.1	7	12.1	--	--	--	--	8.47	8.29	4	--	17
Tm	1	0.5	1	0.8	1.5	--	--	--	--	0.96	1.03	1	--	1.8
Yb	6.8	3	5.6	5.2	8	5.72	6.18	2.87	3.82	5.3	5	5	9.5	15.5
Lu	0.7	0.3	0.8	0.7	1	--	--	--	--	0.75	0.6	0.7	0.08	--

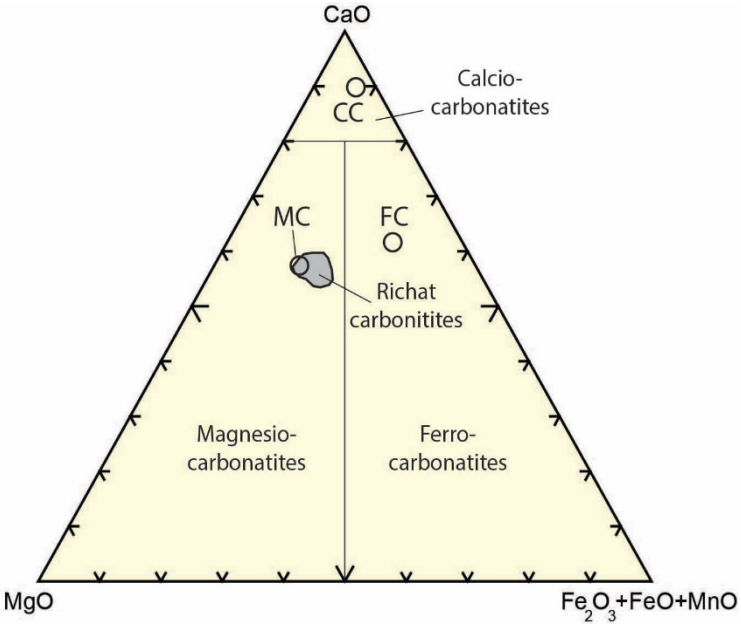

Figure 10. Carbonatite classification diagram of Woolley (1982). Richat data is from table 3.

The carbonatites are composed predominantly of dolomite and ankerite with abundant apatite, and lesser amounts of magnetite, and barite (Woolley and others, 1984, Matton and Jébrak, 2008). Sparse micron-sized brown crystals are interpreted to be pyrochlore (Woolley and others, 1984). Apatite is abundant as stubby subhedral somewhat rounded prisms. Fission-track dating of the apatite by Poupeau and others (1996) indicates a Cretaceous age of 99±5 Ma.

Unexposed kimberlitic rocks in the form of plugs and sills underlie a small area at the northwestern margin of the structure (fig. 8; Matton and others, 2005). According to Matton and Jébrak (2008) the kimberlite was examined by Asthon Mining Inc., who report an approximate age of 99 Ma. No details about the results of the Asthon Mining investigation or basis for the age are given. Matton and others (2005) indicate that a magnetic anomaly is associated with the kimberlite and that may have been the basis for its discovery. The kimberlite is weathered and composed of phlogopite with lesser amounts of pyroxene, olivine, amphibole and alteration minerals (serpentinite, smectite, chlorite, magnetite, and hematite). Gunn and others (2004) report that two kimberlite provinces have been found apparently spatially associated with a major WSW-ENE lineament within the Taoudeni Basin outside the BGS study area. The western cluster is located near the Guelb er Richat dome (fig. 8). The eastern cluster contains at least 21 kimberlites, of which seven are diamondiferous.

A small circular plug, formerly interpreted as analcime-bearing sodically altered sedimentary rocks (Boussaroque, 1975), is present on the south-southwestern side of a 5-kilometer-diameter ring of siliceous breccia and reinterpreted as a hydrothermally altered diatreme pipe or maar by Matton and others (2005) (fig. 8). A small volcano-sedimentary basin containing conglomeratic and tuffaceous rocks is present on the north-northeast side of the siliceous breccia and is thought to represent the remnants of a maar deposit. These rocks are rich in the zeolite mineral analcime and, where dominantly composed of this mineral, have been called analcimolite (Bardossy and others, 1963). Dietz and others

(1969) interpreted these rocks as zeolitized volcanic tuffs. Matton and Jébrak (2008) extend this interpretation and conclude they are altered rhyolitic volcanic rocks. These rocks are all sufficiently altered that their original chemistry cannot be properly determined. The volcanic rocks in the core of the structure have not been dated.

The center of the structure is occupied by a siliceous polymictic breccia approximately 3 km in diameter and 40 m thick, thinning to less than a few meters at its margins. The breccia occurs within Proterozoic sedimentary rocks between a partially dolomitized limestone and an overlying sandstone unit. Clasts consist of the locally derived sedimentary rocks and exhibit bimodal sizes and textures indicating solution-rounding and dissolution by hydrothermal fluids followed by internal sedimentation and collapse into voids of the overlying rocks. The breccia is intensely silicified and replaced by microcrystalline quartz with lesser calcite and ankerite (fig. 9D). Vuggy open space within the breccia is filled with microcrystalline quartz and internal sediments suggesting karst type solution cavities (Matton and Jébrak, 2008). Field relationships show that the base of the limestone unit is dolomitized, pyritized, and cut by veins up to several cm thick containing microcrystalline quartz. Woolley and others (1984) noted that barite mineralization was common throughout the breccia and one of our two samples (CT07RIM45-1) contains over 10,000 pm barium (table 1). $^{40}Ar/^{39}Ar$ dating of quartz-potassium feldspar-bearing internal sediments yielded an age of 98.2±2.6 Ma suggesting that emplacement of alkaline intrusive rocks was nearly synchronous with emplacement and silicification of the breccia (Matton and others, 2005). Two specimens collected from chert breccias northwest of the dome center exhibited high P_2O_5 values, the highest consistent with 30–35 volume percent apatite. REE analyses of carbonate show abundances 100 times higher than average sedimentary limestone and are light REE enriched with steep LREE patterns typical of carbonatite.

Matton and others (2005) and Matton and Jébrak (2008) interpret the Richat structure as being formed by early domal uplift by an underlying mafic intrusion that later resulted in a collapse caldera (fig. 12). The early mafic magma is represented by the gabbro ring dikes which were emplaced during doming and emplacement of the intrusion. They propose that the underlying mafic magma chamber then differentiated to form an upper evolved granitic zone that ultimately lead to formation of a collapse caldera. Late in the sequence, upwards migration of hydrothermal fluids from the evolving magma chamber led to formation of the core zone breccia and other hydrothermal alteration events within the structure. Rhyolitic volcanics were erupted during caldera collapse and altered by post collapse hydrothermal fluids. They interpret the eruption of the rhyolite as the last magmatic event within the Richat structure although the basis for this interpretation is unclear. If this is so, then the carbonatites and probably the kimberlites were emplaced after the core intrusion was emplaced but coeval with evolution of the magma chamber at around 99 Ma. The apparent age of formation of the breccia at 98.2±2.6 Ma does support the emplacement of all the Richat magmatic rocks within a fairly short period.

Woolley and others (1984) interpreted the doming of the Richat structure to emplacement of an underlying alkaline igneous intrusive complex. The interpretation of Matton and others described above (Matton and others, 2005; Matton, 2008; Matton and Jébrak, 2008), however, indicates the presence of a possibly non-alkaline intrusive complex beneath the central part of the dome. The presence of the tholeiitic gabbro ring

dikes is good evidence that at least early intrusive activity beneath the dome was non-alkaline although it is possible that a peralkaline granitic magma formed in the upper part of the magma chamber. Even if the core intrusive complex is non-alkaline, the presence of the carbonatite dikes still suggests the possibility of carbonatite and associated alkaline intrusives beneath the southern and western parts of the structure. The co-location of Guelb er Richat on prominent ENE trending structures with two separate swarms of kimberlite intrusions suggests that this structure is seated in the sub-Taoudeni cratonic basement and could localize the emplacement of additional carbonatite and kimberlite bodies.

Although the carbonatite dikes exposed at the surface of the Guelb er Richat dome are not likely to represent an economic target for U, Th, REE resources, they are strong indicators of the possibility that a carbonatite intrusion lies beneath the dome that could be permissive of significant deposits of U, Th, REE, Nb, Ta, Ce, fluorite, and other incompatible elements. Based on similarity to Guelb er Richat, the Semsiyat structure may also represent a carbonatite at depth. The alignment of these possible carbonatites along a northeast trending structure thought to intersect the Birimian aged basement beneath the Taoudeni Basin sediments and associated with two kimberlite swarms, suggests that the northern margin of the Taoudeni Basin along the trend of this structure must be considered permissive of additional carbonatite hosted occurrences of U, Th, Nb, Ta, REE, and fluorite.

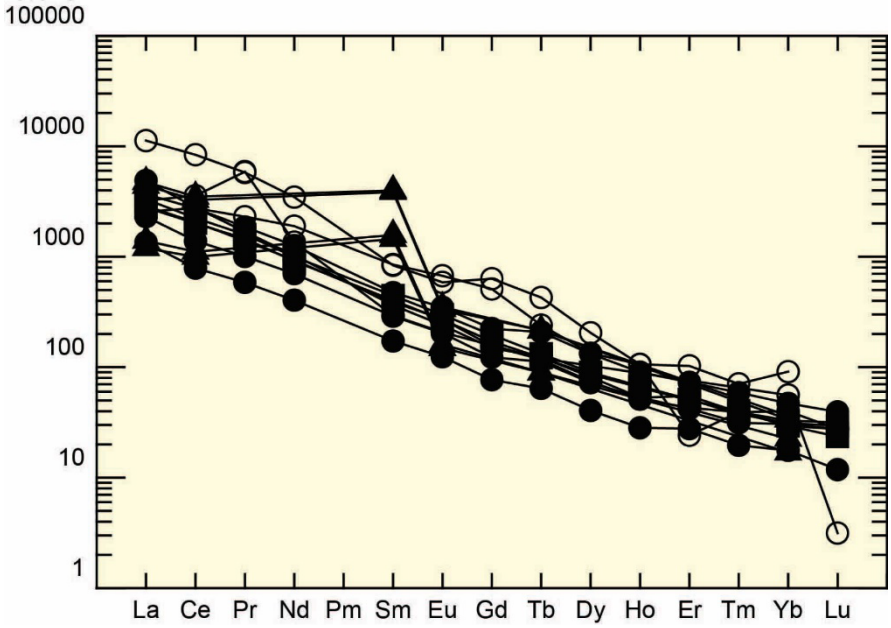

Figure 11. Chonderite normalized REE plot using normalization of Sun and McDonald (1989). Data from tables 1 and 3 (open circles carbonatite averages of Woolley and Kempe (1989), solid circles data of Matton (2008), triangles data of Woolley and others (1984) and squares USGS data).

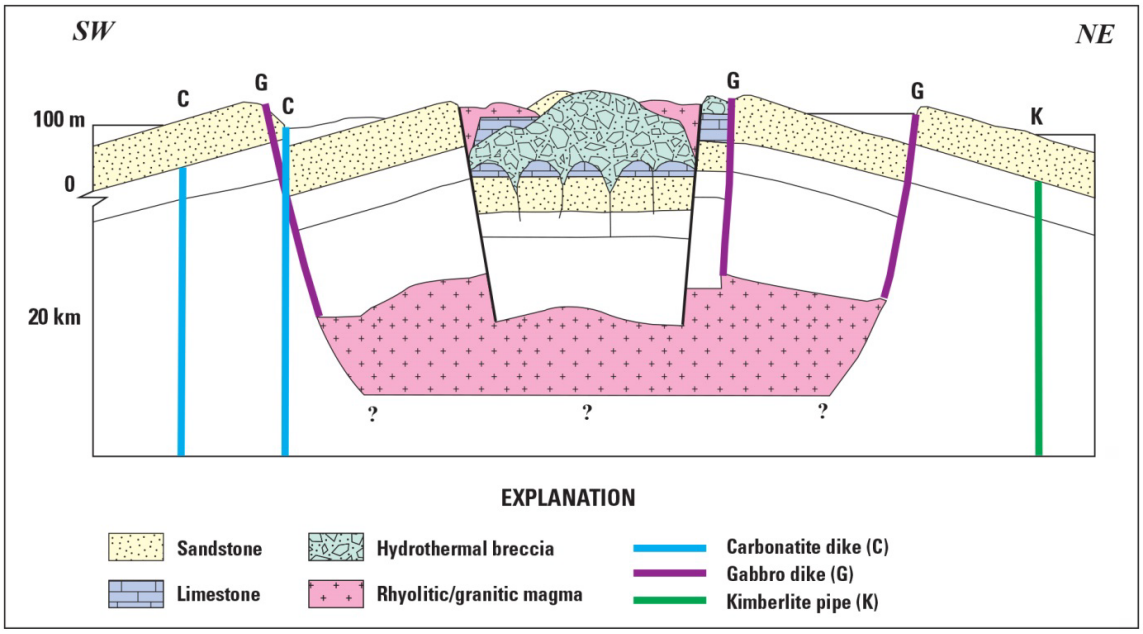

Figure 12. Interpreted collapse caldera cross-section of the Guelb er Richat structure (modified from Matton and Jébrak, 2008.) Purple G = gabbro dike, blue C = carbonatite dike, and green K = kimberlite pipe.

5 Permissive Tracts for Incompatible Element Deposits in Pegmatites, Alkaline Rocks and Carbonatites in Mauritania

Tracts considered permissive for deposits classified as U-Th-REE and other incompatible element deposits in alkaline rocks and carbonatites are shown on figure 13. Criteria for the delineation of these tracts are based upon permissive geology as described in BGS and BRGM reports and summarized above, and are broken out at the group, complex, or suite level. A second major criterion for selection of tracts is the distribution of known occurrences of beryllium, fluorine, REEs, uranium, and thorium where they are hosted within permissive host rocks. Five tracts are defined as follows: in the southwestern Rgueïbat Shield, (1) a tract is drawn as permissive of pegmatite-hosted deposits based upon Mesoarchean supracrustal rocks of the Lebzenia Group, the Tasiast Suite, and the undivided mafic metavolcanic rocks and amphibolites of the LbB unit. Outlines of the greenstone belts were extended using the aeromagnetic response of banded iron formation in the mafic metavolcanic rocks as a proxy for the location of the belts under cover. Although most of the known pegmatite occurrences in this region are located in the Chami and Sebkhet Nich greenstone belts, all of the greenstone belts in the region are permissive of additional pegmatite deposits. (2) A second tract permissive of pegmatite deposits in the Choum Rag el Abiod terrane is drawn on the rocks of the Amsaga Complex. Within this tract, favorable units consist of the amphibole-garnet bearing, granitic gneiss and migmatite of the Tamagot orthogneiss, hypersthene bearing migmatitic gneiss at Guelb el Azid and metagabroic rocks of the Iguilid massif. (3) A

third tract is drawn upon the rocks of the alkaline Tigsmat el Khadra Suite of the northern and eastern Rgueïbat Shield. (4) A fourth tract of major importance is drawn upon the Bou Naga alkaline intrusive complex consisting of quartz syenites and alkaline granites of the central intrusive complex and the surrounding Oued Tidoumaline Formation consisting of the outflow sheets and peripheral pyroclastic deposits of a rhyodacitic volcano. (5) A fifth tract permissive of carbonatite related deposits is currently drawn upon the surface expression of the Guelb er Richat and Semsiyat structures.

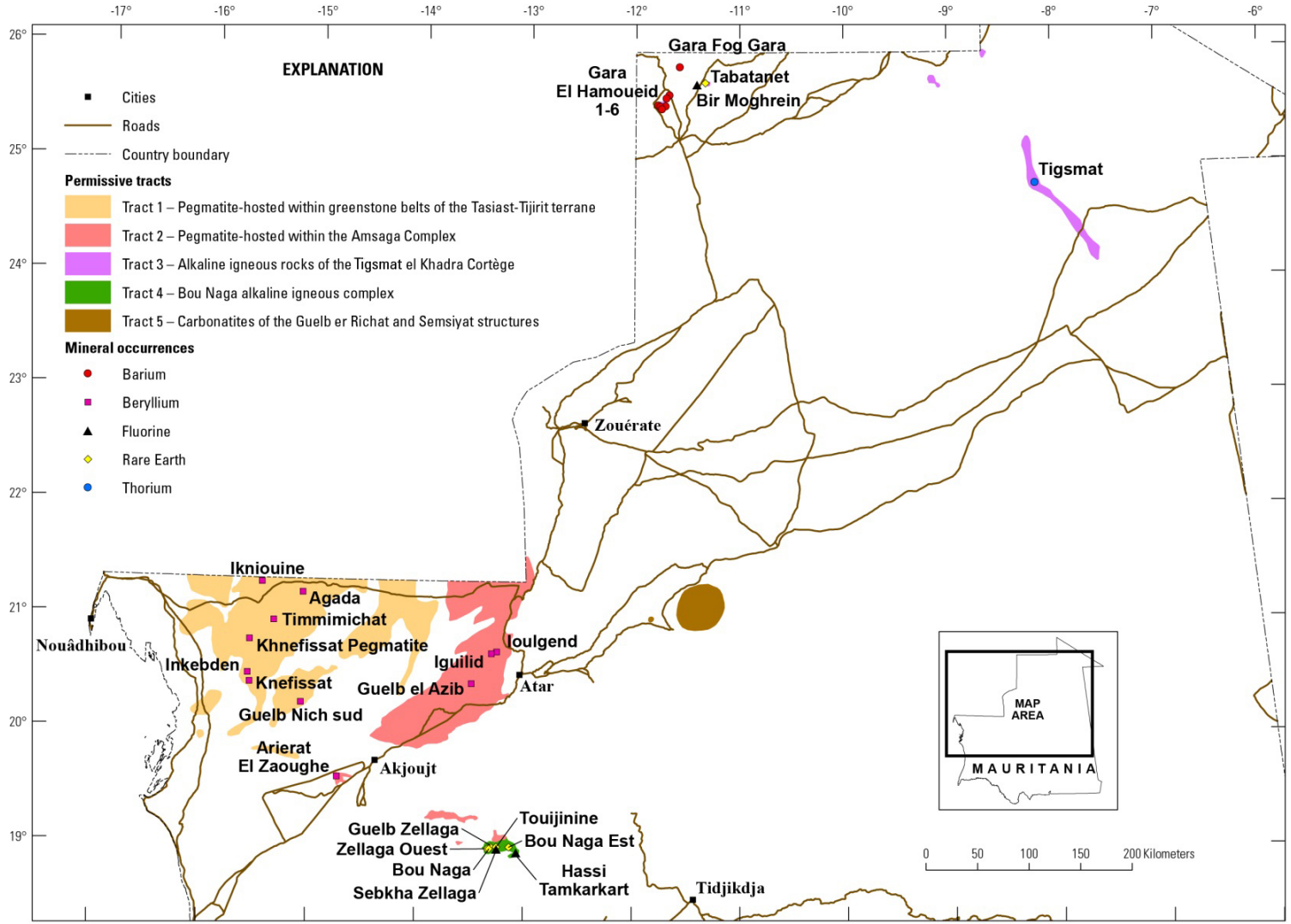

Figure 13. Permissive tracts for U, Th, REE and other incompatible element deposits in pegmatites, alkaline rocks, and carbonatites in Mauritania.

6 Conclusions

Potential for U-Th-REE deposits in alkaline rocks and carbonatite deposits in Mauritania exists within volcano-sedimentary sequences: (1) the Tasiast-Tijirit terrane and the Amsaga Complex of the southwestern Rgueïbat Shield, within the alkaline Tigsmat el Khadra of the northern and eastern Rgueïbat Shield; (2) the Bou Naga alkaline complex of central Mauritania; and (3) at the Guelb er Richat and Semsyat structures along an ENE trending basement structure beneath sediments of the northern Taoudeni Basin margin. Five permissive tracts have been drawn based upon permissive geology at the group level and upon the distribution of known occurrences thought to belong to the U-Th-REE and other incompatible element deposits in pegmatite, alkaline igneous rock and carbonatite classes of deposits.

7 References

Bardossy, G., Monod, T., and Pomerol, C., 1963, Decouverts d'analcimolites d'origine endogene dans les Richat (Adrar Mauritanien): Acad. Sci. Comptes rendus, v. 256, no. 9, p. 3934–3936.

Blanc, A. 1986, Le magmatisme du complexe alcalin minéralisé en terres rares, yttrium, et thorium de Bou Naga (Mauritanie)—Environnement géologique et géochimique, radiochronologie et signification géodynamique: Ph.D. dissertation, Univ. Nice, 313 p.

Blanc, A., Bernard-Griffiths, J., Caby, Renauld, Caruba, Christiane, Caruba, Raoul, Dars, Réné, Fourcade, Serge, and Peucat, J.J., 1992, U-Pb dating and isotopic signature of the alkaline ring complexes of Bou Naga (Mauritania)—Its bearing on late Proterozoic plate tectonics around the West African Craton: Journal of African Earth Sciences, v. 14, no.3, p. 301–311.

Blanc, A., Caruba, Christiane, Caruba, Raoul, Dars, Réné, and Ohnenstetter, D., 1985, The alkaline complex of Bou Naga (Mauritania), Communication: Strasbourg (France), European Union of Geosciences (EUG) III,: Terra Cognita, v. 5, p. 318.

Blanc, A., Caruba, Christiane, Caruba, Raoul, Dars, Réné, Ohnenstetter, D., and Peucat, J.J., 1986, Age archéen du socle de la fenêtre de Bou Naga (Mauritanie): age pan-africain des massifs alcalins intrusifs, in Reunion Annuelle des Sciences de la Terre, v. 11, p. 19.

Blanc, A., and Pomerol, C., 1973, Petrographie des Richat, C—Etude petrographique des roches magmatiques, des filons carbonates et des analcimolites des Richat: Sci. Terre Mem., v. 28, p. 107–134.

Boussaroque, J.L., 1975, Etude des analcimolites des Richat (Adrar de Mauritanie): Ph.D. dissertation, Universite de Paris, 105 p.

Dallmeyer, R.D., and Lécorché, J.-P., 1989, $^{40}Ar/^{39}Ar$ polyorogenic mineral age record within the central Mauritanide orogen, West Africa: Bulletin of the Geological Society of America, v. 101, p. 55–70.

Dietz, R.S., Fudali, Robert, and Cassidy, William, 1969, Richat and Semsiyat domes (Mauritania)—Not astroblemes: Bulletin of the Geological Society of America, v. 80, p. 1367–1372.

Eppinger, R.G., Giles, S.A., Lee, G.K., and Smith, S.M., 2015, Database creation, data quality assessment, and geochemical maps (phase V, deliverable 59)—Final report on

compilation and validation of geochemical data, chap. D *of* Taylor, C.D., ed., Second projet de renforcement institutionnel du secteur minier de la République Islamique de Mauritanie (PRISM-II): U.S. Geological Survey Open-File Report 2013–1280-D, 52 p., http://dx.doi.org/10.3133/ofr20131280/. [In English and French.]
Fudali, R.F., 1969, Coesite from the Richat Dome, Mauritania—A misidentification: Science, p. 228–230.
Gunn, A.G., Pitfield, P.E.J., Mckervey, J.A., Key, R.M., Waters, C.N., and Barnes, R.P., 2004, Notice explicative des cartes géologiques et gîtologiques à 1/200 000 et 1/500 000 du Sud de la Mauritanie, Volume 2—Potentiel Minier: Direction des Mines et de la Géologie (DMG), Ministère des Mines et de l'Industrie, Nouakchott.
Lahondère, D., Thieblemont, D., Goujou, J.-C., Roger, J., Moussine-Pouchkine, A., LeMetour, J., Cocherie, A., and Guerrot, C., 2003, Notice explicative des cartes géologiques et gîtologiques à 1/200 000 et 1/500 000 du Nord de la Mauritanie—Volume 1: Direction des Mines et de la Géologie (DMG), Ministère des Mines et de l'Industrie, Nouakchott.
Matton, Guillaume, Jébrak, Michel, and Lee, J.K.W., 2005, Resolving the Richat enigma—Doming and hydrothermal karstification above an alkaline complex: Geology, v. 33, no. 8, p. 665–668.
Matton, Guillaume, and Jébrak, Michel, 2008, The "Eye of Africa" (Richat Dome, Mauritania)—An isolated Cretaceous alkaline-hydrothermal complex, chap. II, *in* The Cretaceous Richat Complex (Mauritania)—A peri-Atlantic alcaline process: Montréal, Canada, Université du Québec, Ph.D. dissertation, p. 30–72.
Matton, Guillaume, 2008, The Cretaceous Richat Complex (Mauritania)—A peri-Atlantic alcaline process: Montréal, Canada, Université du Québec, Ph.D. dissertation, 154 p.
Marcellin, J., 1965, Etude de la série d'Akjoujt dans l'Inchiri (campagne 1963–1964): Dakar, Rapp. inéd. Bur. Rech. géol. min., Rapport DAK 65-A9, 59 p.
Marot, A., Stein, G., Artigan, D., and Milési J.-P., 2003, Notice explicative des cartes géologiques et gîtologiques à 1/200 000 et 1/500 000 du Nord de la Mauritanie, Volume 2 – Potentiel Minier, DMG, Ministère des Mines et de l'Industrie, Nouakchott.
Marsh, E.E., and Anderson, E.D., 2015, Database of mineral deposits in the Islamic Republic of Mauritania (phase V, deliverables 90 and 91), chap. S *of* Taylor, C.D., ed., Second projet de renforcement institutionnel du secteur minier de la République Islamique de Mauritanie (PRISM-II): U.S. Geological Survey Open-File Report 2013–1280-S, 9 p., Access database, http://dx.doi.org/10.3133/ofr20131280/. [In English and French.]
Mining Annual Review, 1968–1970, Mauritania—Mining Annual Review 1968, 1969, 1970: London, Mining Journal Ltd.
O'Connor, E.A., Pitfield, P.E.J., Schofield, D.I., Coats, S., Waters, C., Powell, J., Ford, J., Clarke, S., and Gillespie, M., 2005, Notice explicative des cartes géologiques et gîtologiques à 1/200 000 et 1/500 000 du Nord-Ouest de la Mauritanie: Direction des Mines et de la Géologie (DMG), Ministère des Mines et de l'Industrie, Nouakchott.
Pitfield, P E J., Key, R M., Waters, C N., Hawkins, M.P.H., Scholfield, D.I., Loughlin, S. and Barnes, R P., 2004. Notice explicative des cartes géologiques et gîtologiques à 1/200 000 et 1/500 000 du Sud de la Mauritanie. Volume 1—géologie. Direction des Mines et de la Géologie (DMG), Ministère des Mines et de l'Industrie, Nouakchott.

Pouit, G., 1968, Le gisement de Terres-Rares (Y) de Bou Naga (R.I.M.): Départment des Mines et Géologie (R.I.M.), 20 p.
Poupeau, G., Fabre, J., Labrin, E., Azdimoussa, A., Netto, A.M., and Monod, T., 1996, Nouvelles datations par traces de fission de la structure circulaire des Richat (Mauritanie): Memoires du Service Geologique de l'Algerie, v. 8, p. 231–236.
Rocci, G., 1957, Formations métamorphiques et granitiques de la partie occidentale du pays Rgueïbat (Mauritanie du Nord): Bulletin de la Direction Federale des Mines et de la Geologie, no. 21, Tome 1, Gouvernement General de l'Afrique Occidentale Francaise, 303 p.
Rocci, G., 1960, Sur un nouvel affleurement de roches hyperalcalines dans l'ouest Africain le massif de Tabatanat en Mauritanie septentrionale: Ann. Fac. Sci. Univ., Dakar, 5, p. 25–33.
Sun S.-S., and McDonough, W.F., 1989, Chemical and isotopic systematics of oceanic basalts—Implications for mantle composition and processes, *in* Saunders, A.D., and Norry, M.J., eds., Magmatism in the Ocean Basins: Geological Socociety, London, Special Publublication 42, p. 313–345.
Taylor, C.D., ed., 2007, Phase I summary report—USGS Evaluation of PRISM-I Data: U.S. Geological Survey, Administrative Report to DMG: Direction des Mines et de la Géologie (DMG), Ministère des Mines et de l'Industrie, Nouakchott, 107 p.
Trompette, R., 1963, Mission Akjoujt 1962–63, Reconnaissance géologique du Tamkarkart: Bureau de Recherches Géologiques et Minières (BRGM), Dakar, Rapport DAK 63-A20, 51 p.
Van Alstine, R.E., and Schruben P.G., 1980, Fluorspar resources of Africa: U.S. Geological Survey Bulletin 1487, 25 p.
Woolley, A.R., 1982, A discussion of carbonatite evolution and nomenclature, and the generation of sodic and potassic fenites: Mineralogical Magazine, v. 46, p. 13–17.
Woolley, A.R., and Kempe, D.R.C., 1989, Carbonatites—Nomenclature, average chemical compositions, and element distribution, *in* Bell, Keith, ed., Carbonatite: Genesis and Evolution: London, Unwin Hyman, Ltd, p. 1–14.
Woolley, A.R., Rankin, A.H., Elliott, C.J., Bishot, A.C., and Niblett, D., 1984, Carbonatite dykes, from the Richat dome, Mauritania, and the genesis of the dome: The Indian Mineralogist, p. 189–207.

ISSN 2331-1258 (online)
http://dx.doi.org/10.3133/ofr20131280